Electronegative LDL circulating in smokers impairs endothelial progenitor cell differentiation by inhibiting Akt phosphorylation via LOX-1

Daming Tang,* Jonathan Lu,* Jeffrey P. Walterscheid,* Hsin-Hung Chen,* David A. Engler,† Tatsuya Sawamura,§ Po-Yuan Chang, Hazim J. Safi,†† Chao-Yuh Yang,* and Chu-Huang Chen[1,*]**

Department of Medicine,* Baylor College of Medicine, Houston, TX; Department of Internal Medicine,† University of Texas-Houston Medical School, Houston, TX; National Cardiovascular Research Institute,§ Suita, Osaka, Japan; Departments of Internal Medicine,** National Taiwan University Hospital and National Taiwan University College of Medicine, Taipei, Taiwan; and Department of Cardiothoracic and Vascular Surgery,†† University of Texas-Houston Medical School, Houston, TX

Abstract Endothelial progenitor cells (EPCs), important for endothelial regeneration and vasculogenesis, are reduced by cigarette smoking. To elucidate the mechanisms, we examined the effects of electronegative LDL, circulating in chronic smokers, on EPC differentiation. Using ion-exchange chromatography, we purified smoker LDL into five subfractions, L1–L5. In matched, nonsmoking healthy subjects, L5, the most electronegative subfraction, was either absent or scanty. Sustained L5 treatment inhibited CD31 and KDR expression and EPC differentiation, whereas L1–L4 had no effect. L5 also inhibited telomerase activity to accelerate EPC senescence in correlation with reduced Akt phosphorylation. Transfection of day 3 EPCs with dominant negative Akt constructs inhibited CD31 and KDR expression, stalled EPC differentiation, and promoted early senescence. In contrast, transfection with constitutively active Akt rendered the EPCs resistant to L5, allowing normal maturation. L5 upregulated the lectin-like oxidized low density lipoprotein receptor 1 (LOX-1), and pretreatment of EPCs with TS20, a LOX-1-neutralizing antibody, blocked internalization of L5 by EPCs and prevented L5-mediated inhibition of EPC differentiation. Mixing L5 with L1 to physiological L5/L1 ratios did not attenuate L5's effects. These findings suggest that cigarette smoking is associated with the formation of L5, which inhibits EPC differentiation by impairing Akt phosphorylation via the LOX-1 receptor.—Tang, D., J. Lu, J. P. Walterscheid, H-H. Chen, D. A. Engler, T. Sawamura, P-Y. Chang, H. J. Safi, C-Y. Yang, and C-H. Chen. **Electronegative LDL circulating in smokers impairs endothelial progenitor cell differentiation by inhibiting Akt phosphorylation via LOX-1.** ***J. Lipid Res.*** **2008.** 49: **33–47.**

Supplementary key words electronegative low density lipoprotein • L5 • lectin-like oxidized low density lipoprotein receptor 1 • signal transduction

Atherosclerosis is an inflammatory disease; one of its earliest manifestations is endothelial dysfunction. Replication of neighboring endothelial cells (ECs) was long thought to be the chief or sole mechanism for replacing damaged ECs (1). However, increasing data now support bone marrow-derived endothelial progenitor cells (EPCs) as playing a key role in endothelial regeneration as well as in vasculogenesis (2–5). EPCs have been shown to be reduced in number and/or functional activity in the presence of traditional and emerging major risk factors, whether severally or as clusters (6). Reported relations include those with aging (7), subclinical and clinical atherothrombotic disease (8, 9), type 1 and type 2 diabetes mellitus (10, 11), hypercholesterolemia (12), smoking (6), C-reactive protein increase (13), and the metabolic syndrome (14).

The mechanism of tobacco's effects on EPCs is unknown. Michaud et al. (15), in an initial study, found the EC-specific markers vascular endothelial cadherin, vascular endothelial growth factor (VEGF) receptor 2 (VEGFR2; also known as KDR), and von Willebrand factor (vWF) to be reduced and the formation of reactive oxygen species to be increased in EPCs from smokers. The known effects of nicotine on postnatal vasculogenesis (16) may be mediated in part by the mobilization of EPCs (17). Whereas

Abbreviations: AcLDL, acetylated low density lipoprotein; Akt-CA, plncx-HA-myr-Akt (constitutively active Akt); Akt-DN, plncx-HA-myr-Akt179M (dominant negative Akt); DiI, 1,1′-dioctadecyl-3,3,3′,3′-tetramethylindocarbocyanine; EC, endothelial cell; EGF, epidermal growth factor; EPC, endothelial progenitor cell; LOX-1, lectin-like oxidized low density lipoprotein receptor 1; MTS, 3-(4,5-dimethylthiazol-2-yl)-5-(3-carboxymethoxyphenol)-2-(4-sulfophenyl)-2H-tetrazolium; OxLDL, experimentally oxidized low density lipoprotein; SA-β-gal, senescence-associated β-galactosidase; VEGF, vascular endothelial growth factor; vWF, von Willebrand factor.

[1] To whom correspondence should be addressed.
e-mail: cchen@bcm.tmc.edu

Manuscript received 3 July 2007 and in revised form 19 September 2007.

Published, JLR Papers in Press, October 1, 2007.
DOI 10.1194/jlr.M700305-JLR200

nicotine is cytotoxic at high concentrations, at low concentrations it increases EPC number and activity (18).

In the current study, we hypothesized that smoking's effects on EPCs are, at least in part, lipid-mediated. It is well established that smoking and dyslipidemia increase the risk for coronary artery and peripheral vascular disease synergistically. Cigarette smoke extracts such as acrolein and other gas-phase oxidants (19) increase superoxide anion (20) by stimulation of NADPH (19), which in turn inhibits reactive oxygen species function with a reduction of nitric oxide production and bioactivity (21) and results in impaired endothelium-dependent vasodilation (22) and direct cell death (23). Moreover, cigarette smoke is a source of free radicals that lead to oxidative stress and depletion of antioxidants, including vitamin C, carotene, and folate (24–26). The increased oxidants in smokers act directly to depress nitric oxide production by the endothelium, independent of any effect on mitochondrial respiration.

Besides directly damaging the endothelium, cigarette smoke can adversely modify lipoproteins and make them atherogenic through oxidation of their apolipoprotein (27) and lipid (28) components. By increasing cholesterol oxidation and lipid peroxidation, cigarette smoke extracts can reduce the affinity of human LDL to LDL receptors on hepatocytes (28). Cigarette smoke-modified LDL showed higher anodic electrophoretic mobility (28), implicating cigarette smoke in the generation of electronegative LDL through mechanisms yet to be elucidated. We previously showed that L5, a highly electronegative LDL, was present in nonsmoking hypercholesterolemic subjects (29). Here, we report on L5 in the plasma of chronic smokers without increased LDL-cholesterol. In addition to their role in the replacement of ECs in macrovessels, EPCs are now considered contributory to the building of microvessels and neovascularization in ischemic or damaged tissues (4, 5, 30). The focus of the current study is whether and how smoker L5 inhibits EPC differentiation at an early stage.

Akt, a family member of serine/threonine protein kinases, is closely linked to neovascularization through a variety of stimuli in ECs and EPCs, including the promotion of EC survival and migration and nitric oxide production (2, 31–33). Dominant negative Akt (Akt-DN) overexpression leads to functional interruption of EPC bioactivity (34). Recent studies showed that experimentally (copper) oxidized low density lipoprotein (OxLDL) inhibits VEGF-induced EPC differentiation through dephosphorylation of Akt and accelerates the onset of EPC senescence (35, 36). Here, we provide evidence derived from the naturally modified L5 to support the observations made with experimentally prepared OxLDL.

Since its cloning by Sawamura and colleagues (37), lectin-like oxidized low density lipoprotein receptor (LOX-1) has been well characterized in its role in transducing the signaling of copper-OxLDL. Previous studies showed that OxLDL can enhance LOX-1 expression in both EPCs (36, 38, 39) and human ECs (40, 41). In this study, we examined how smoker L5 may affect EPC differentiation through this receptor.

METHODS

Preparation of LDL

Total LDL (density = 1.019–1.063 g/ml) was separated from normal human plasma by ultracentrifugation (29). All reagents were purchased from Sigma-Aldrich Biotechnology. To minimize in vitro oxidation and microorganism contamination, the plasma was adjusted to contain 100 μM EDTA, 0.056 U/ml aprotinin, 0.06% sodium azide, and 50 μg/ml gentamycin. Protein concentrations were determined using the modified Lowry assay method.

LDL subfractionation

Fasting blood samples were obtained from six smokers and six healthy, nonsmoking subjects (three males and three females, age 30–48 years, both groups). All smokers consumed one to two packs of cigarettes per day, and each had at least 1.5 years of continuous smoking history. Written approval was received by the Baylor College of Medicine Institutional Review Board and an informed consent was signed by all study subjects. All subjects were normocholesterolemic, with LDL cholesterol 9 120 mg/dl (means ± SEM, 110 ± 8 and 110 ± 7 mg/dl; $P > 0.01$). Plasma triglyceride was <180 mg/dl in all subjects, none of whom had a history of diabetes mellitus, hypertension, clinical manifestations of atherothrombotic disease, or any other systemic disorder.

The LDL fractions were separated using UNO Q12® ion-exchange columns (Bio-Rad Laboratories) and two Pharmacia P-500 HPLC pumps with a Pharmacia LCC-500 controller (42). The columns were preequilibrated with buffer A (0.02 M Tris HCl, pH 8.0, and 0.5 mM EDTA) in a 4°C cold room. Subfractions were eluted by the use of a multistep gradient of buffer B (1 M NaCl in buffer A). Samples equilibrated with buffer A were eluted with a linear gradient program at a flow rate of 2 ml/min. The effluent was monitored at 280 nm and protected from ex vivo oxidation with 5 mM EDTA. The LDL fractions were concentrated with Centriprep® filters (YM-30; Millipore Corp.) and sterilized by passing through 0.20 μm filters. The isolated fractions were stored at 4°C while samples were being characterized.

Isolation and cell culture of EPCs

Circulating mononuclear cells were isolated fresh from normolipidemic peripheral blood donations from nonsmokers, then cultured as described previously (2). In brief, mononuclear cells were separated from other components in the buffy coat by centrifugation using Histopaque®-1077 density-gradient tubes (Sigma-Aldrich Biotechnology). After three washings with PBS, 1×10^6 purified mononuclear cells were seeded on 2% gelatin-coated six-well plates. Cells were cultured in EC basal medium 2 (EBM-2®; Clonetics) supplemented with the EGM-2-MV Bullet-Kit® (Clonetics), containing 5% FBS, 50 ng/ml VEGF (R&D Systems), 50 ng/ml human fibroblast growth factor 2 (R&D Systems), human epidermal growth factor (EGF), insulin-like growth factor 1, and ascorbic acid.

EPCs were defined by the expression of EC lineage markers, including vWF, KDR, and CD34 (35). Adherent cells at day 3 were rinsed with HBSS and immediately fixed with 4% paraformaldehyde for 10 min at 37°C. Direct and indirect immunostainings were performed with the use of EC-specific antibodies directed against vWF (GeneTex, Inc.), KDR, CD31, and CD34 (BD Pharmingen™, BD Biosciences). Detection of KDR required permeabilization by a 10 min incubation with 0.1% Triton® X-100 (Sigma-Aldrich Biotechnology). Staining of biotin-conjugated mouse anti-human KDR (Sigma-Aldrich Biotechnology) was visualized using streptavidin-FITC conjugate (BD Pharmingen™, BD Biosciences). The anti-CD31, anti-CD34, and anti-vWF anti-

bodies were linked directly to FITC-phycoerythrin (BD Pharmingen™, BD Biosciences). As a negative control, we used nonspecific antibodies of the same isotypes and species. After staining, cells were viewed with an inverted fluorescence microscope (Carl Zeiss MicroImaging) using standard FITC and phycoerythrin excitation and emission filter combinations. Additional confirmation was made by internalization of LDL or acetylated low density lipoprotein (AcLDL; Invitrogen) labeled, as described (35), with 1,1′-dioctadecyl-3,3,3′,3′-tetramethylindocarbocyamine perchlorate (DiI). The medium was changed and adherent cells were washed with medium and incubated with 2.4 μg/ml DiI-labeled LDL or DiI-labeled AcLDL for 1 h before microscopy.

RNA preparation and RT-PCR

RNA preparation with purification of total RNA was performed using the RNeasy® Mini Kit (Qiagen, Inc.), including a DNase step. In brief, cells were lysed in guanadinium isothiocyanate buffer and RNA was purified according to the manufacturer's instructions. The purified RNA was suspended in diethyl pyrocarbonate-treated water. To generate cDNA, 1 μg of total RNA was treated with DNase I (Ambion, Inc.) to remove any contaminating genomic cDNA. The first strand of cDNA was synthesized using the SuperScript® First-Strand Synthesis System for RT-PCR (Invitrogen). The transcribed cDNA was then used for PCR amplification to estimate the expression of LOX-1. RT-PCR was conducted using the Qiagen two-step RT-PCR kit. Human LOX-1 primers were 5′-GAAACTGGAGGGACAGATCTC-3′ (forward) and 5′-CGCATAAACAGCTCCTCGTTG-3′ (reverse), and human GAPDH primers were 5′-ACCACAGTCCATGCCATCAC-3′ (forward) and 5′-TCCACCACCCTGTTGCTGT-3′ (reverse). PCR products were 523 and 484 bp. The thermal cycling conditions were 30 min at 50°C for reverse transcription, 15 min at 95°C for the initial PCR activation step, 30 s at 94°C for cycling denaturation, 30 s at 55°C for annealing, and 30 s at 72°C for extension, each for 30 cycles. The samples were run in a Bio-Rad Thermal Cycler.

Plasmids and transfection

Constitutively active plncx-HA-myr-Akt (Akt-CA) and Akt-DN plasmids were provided by Dr. Marco Marcelli (43). Day 3 EPCs were transfected with Akt-DN and Akt-CA using Lipofectamine™ and PLUS® reagents (Life Technologies). The transfection mixture contained 0.5 μg of plasmid, 4 μl of PLUS®, and 150 μl of EBM® medium (Clonetics) and was incubated for 15 min before application. Cells were washed once with EBM and then incubated with the mixture and 1 ml of EBM for 3 h. Subsequently, 1 ml of EBM was added, and cells were incubated for a further 3 h before the medium was changed. Morphological changes of the cells were documented at 6 h after transfection, and cell differentiation was documented weekly during continuous exposure to 10 μg/ml L1 or L5 in culture medium. For the cell death and proliferation assays, cells were plated at 1×10^4 cells/well onto 96-well plates to allow adherence to dish beds. After another 3 h, the cells were treated with L1 or L5 for 24 h. Before L1 or L5 treatment, serum-free EBM-2® was supplemented with 50 ng/ml VEGF. Whenever pharmacological inhibition of LOX-1 was indicated, we used 10 μg/ml TS20, a LOX-1-neutralizing antibody (developed by T. Sawamura).

Cell death ELISA

Circulating monocytes were seeded at 1×10^6 cells/well onto six-well plates in complete EBM-2® medium as described above. On day 3, after Akt-DN and Akt-CA transfection, cells were replated at 1×10^4 cells/well onto 96-well plates and incubated with L5 at concentrations of 5, 10, 25, and 50 μg/ml for 24 h in EBM-2® medium supplemented with 50 ng/ml VEGF. To further assess the effects of L5 under physiological conditions, additional experiments were performed using a mixture of L5 (1–50 μg/ml, protein concentration) and L1 (500 μg/ml, protein concentration), with a final L5/L1 ratio of 0.2–10%. A quantitative ELISA that detects DNA fragments was used in accordance with the manufacturer's instructions (Cell Death Detection ELISA Kit; Roche Diagnostics) (44). This ELISA detects mononucleosomal and oligonucleosomal DNA using the cytoplasmic fractions of cell lysates. In brief, anti-histone antibody was coated onto a microtiter plate. After a washing step, the wells were incubated with 200 μl of blocking buffer for 30 min and the wells were again washed and incubated with 100 μl of sample for 90 min at room temperature. After another washing step, the wells were incubated with 100 μl of anti-DNA peroxidase for an additional 90 min. The addition of substrate solution produces a color change after 15 min. The color change was compared with a blank well with added substrate. The absorbance was read at 450 nm on an automated ELISA plate reader.

Proliferative activity assay

Mitogenic activity was assayed using a colorimetric MTS [for 3-(4,5-dimethylthiazol-2-yl)-5-(3-carboxymethoxyphenol)-2-(4-sulfophenyl)-2H-tetrazolium] assay kit (CellTiter 96 AQ®; Promega Corp.) (36). EPCs at day 3 after transfection were reseeded on 96-well plates (1×10^4 cells/well) in 0.1 ml of serum-free EBM-2® medium in the presence or absence of 50 ng/ml human VEGF. After 24 h in culture with increasing concentrations of L1 or L5, 20 μl of the combined MTS-phenazine methosulfate solution was added to each well and absorbance at 490 nm was detected with an ELISA plate reader.

β-Galactosidase activity assay

Senescence-associated β-galactosidase (SA-β-gal) activity was measured as described (45). In brief, 24 h after L1 or L5 treatment, untransfected and Akt-CA/Akt-DN-transfected EPCs were washed with PBS and fixed for 5 min in 2% paraformaldehyde at room temperature. They were then washed again and incubated for 16 h at 37°C with fresh SA-β-gal stain solution: 1 mg/ml 5-bromo-4-chloro-3-indyl β-D-galactopyranoside, 5 mM potassium ferrocyanide, 5 mM potassium ferricyanide, 150 mM NaCl, 2 mM $MgCl_2$, 0.01% sodium deoxycholate, and 0.02% Nonidet-40. Finally, the processed EPCs were counterstained with 4′,6-diamino-phenylindole (0.2 μg/ml in 10 mM Tris-HCl, pH 7.0, 10 mM EDTA, and 100 mM NaCl) for 10 min to determine total cell numbers.

Telomeric repeat amplification protocol assay

For quantitative analysis of telomerase activity, the *Telo*TAGGG PCR ELISA^{PLUS} Kit® (Roche Applied Science) was used according to the manufacturer's instructions (46).

Western blotting

EPCs were treated with increasing concentrations of L1 (10 or 500 μg/ml), L5 (1, 5, or 10 μg/ml), or L5 in various concentrations mixed with 500 μg/ml L1, with or without 10 μg/ml TS20 pretreatment, in the presence of 50 ng/ml VEGF. Cellular proteins were prepared and separated on SDS-PAGE gels, as described (29). Membranes were blocked by incubation in Tris-buffered saline (10 mM Tris, pH 7.5, and 100 mM NaCl) containing 0.1% (v/v) Tween-20 and 5% (v/v) nonfat dry milk for 2 h. Specific protein detection was accomplished with mouse polyclonal anti-KDR, anti-CD31 (BD Pharmingen™, BD Biosciences), rabbit polyclonal antiphospho-Akt, anti-Akt (Cell Signal-

ing Technology), or goat polyclonal anti-LOX-1 (GeneTex, Inc.) antibodies. The membranes were washed extensively in Tris-buffered saline containing 0.1% (v/v) Tween-20 before incubation for 1 h with a secondary anti-mouse or anti-rabbit antibody conjugated to horseradish peroxidase. Membranes were then washed and developed using ECL substrate (Amersham Pharmacia Biotech, now GE Healthcare).

Statistical analysis

Data are expressed as means ± SEM. Statistical analysis was performed by one-way ANOVA (least significant difference test) for multiple testing. Probability values were considered significant at $P < 0.05$.

RESULTS

Effects of L5 from smokers on EPC apoptosis and differentiation

L5 was present in all of the plasma LDL samples from smokers but in none from nonsmokers (**Fig. 1A, B**). Smokers' L5 was similar in apoptotic activity to that reported previously for L5 from hypercholesterolemic subjects (29). It induced apoptosis in day 3 EPCs at a concentration of 25 or 50 μg/ml, as assessed by morphological changes of propidium iodide-stained nuclei. It is important to note that L5 at 10 μg/ml or lower did not induce apoptosis. L1 had no apoptotic effect up to the highest concentration (50 μg/ml) examined (Fig. 1C, D).

To confirm that L5 remains unaltered in the milieu of other lipoproteins, we incubated L5 and the most abundant L1 in equal concentrations at 37°C for 24 h and then subjected the mixture to a secondary chromatography. As shown, two discrete spikes representing L1 and L5 reappeared in the second tracing at an interval identical to that of the original tracing (Fig. 1E, F). Of importance, in a mixture containing 500 μg/ml L1, 25–50 μg/ml L5 remained capable of inducing EPC apoptosis, whereas 1–10 μg/ml L5 in the mixture did not (Fig. 1G, H). These findings strongly suggest that although L5 is only a small portion of total LDL, its chemical/physical and functional properties are not compromised by the presence of a large quantity of L1. For most of the subsequent experiments, 1–10 μg/ml L5 (0.2–2% of the quantity of L1) was used to avoid apoptosis.

EPC colonies isolated from human blood buffy coats proliferated and smoothly differentiated into EC sheets, taking on a cobblestone-like appearance in the presence of VEGF after 28 days in culture (**Fig. 2A**). Initially, EPC colonies reorganized as a cell mass composed of a central cord of round cells with elongated, spindle-shaped cells sprouting at the periphery of the colony. By day 3, clusters of round cells that sat on top of spindle-shaped cells migrated from the base of the cell clusters. During the subsequent 2 weeks, the clusters of cells gradually disappeared and the spindle-shaped cells, displaying EC features, were left to adhere to the culture wells. By the 4th week, in the presence of EGF, insulin-like growth factor-1, fibroblast growth factor 2, and VEGF, endothelium-like cells proliferated and aggregated in the familiar cobblestone pattern. Similarly prepared cells have been reported to express KDR, CD31, CD34, and Tie-2 (angiopoietin 1 receptor) (47). As stated above, our cells were able to express KDR, CD34, and vWF and to internalize LDL and AcLDL (Fig. 2B).

Because L5 at concentrations > 10 μg/ml induces EPC apoptosis, we compared the effects of 10 μg/ml total nonsmoker LDL, smoker L1, and smoker L5 on EPC differentiation. As shown in Fig. 2A, neither nonsmoker LDL nor smoker L1 changed the course of EPC differentiation and maturation, compared with PBS treatment. In contrast, cells exposed to this subapoptotic concentration of L5 alone or in a mixture with 500 μg/ml L1 dissociated without proliferation; furthermore, there was an absence of elongated, spindle-like ECs sprouting from the periphery of the colony. At day 28, there was no evidence of cobblestone-like EC aggregates, despite supplementation of 50 ng/ml VEGF.

Effects of L5 on Akt phosphorylation

Because Akt activation is important for EPC differentiation, we examined whether L5 at a low concentration could inhibit Akt phosphorylation at an early stage of differentiation. In day 3 EPCs, L5 alone or in a mixture with 500 μg/ml L1 inhibited Akt phosphorylation in a concentration-dependent manner, without affecting total Akt content. The inhibitory effect was seen at a concentration as low as 5 μg/ml (**Fig. 3A, C**). In comparison, L1 had no effect on Akt phosphorylation (Fig. 3B).

Effects of Akt-DN and Akt-CA expression on EPC apoptosis and differentiation

To examine further the effect of Akt activation on EPC differentiation, we transfected day 3 EPCs with an Akt-DN or Akt-CA plasmid. Akt phosphorylation was reduced in Akt-DN-treated cells compared with untransfected EPCs, whereas it was enhanced in Akt-CA-treated cells (**Fig. 4A**). In the absence of L5, Akt-DN transfection resulted in spontaneous apoptosis in ~35% of EPCs, as shown by propidium iodide nuclear staining, whereas Akt-CA cells appeared healthy (Fig. 4B).

To confirm that the L5-mediated inhibition of EPC differentiation was not a result of apoptosis, the extent of DNA fragmentation was measured by cell death ELISA. At concentrations > 10 μg/ml, DNA fragmentation increased in Akt-DN-transfected EPCs and decreased in Akt-CA-transfected EPCs, compared with native cells (Fig. 4C). The proapoptotic effect of Akt-DN and the antiapoptotic effect of Akt-CA are demonstrated in EPCs treated with L1, which did not affect DNA fragmentation, even at 50 μg/ml. However, spontaneous apoptotic activity was slightly but nonsignificantly increased in Akt-DN-transfected EPCs. The proliferation rate of EPCs was determined to rule out the possibility that the inhibitory effect of L5 on VEGF-induced EPC differentiation was secondary to the induction of apoptosis. In this setting, neither L1 nor L5 at lower concentrations (5 and 10 μg/ml) increased the rate of EPC apoptosis. However, L5 inhibited proliferation in EPCs and Akt-DN-transfected EPCs (Fig. 4D), whereas L5 at 25 and 50 μg/ml yielded an increase in EPC apoptosis

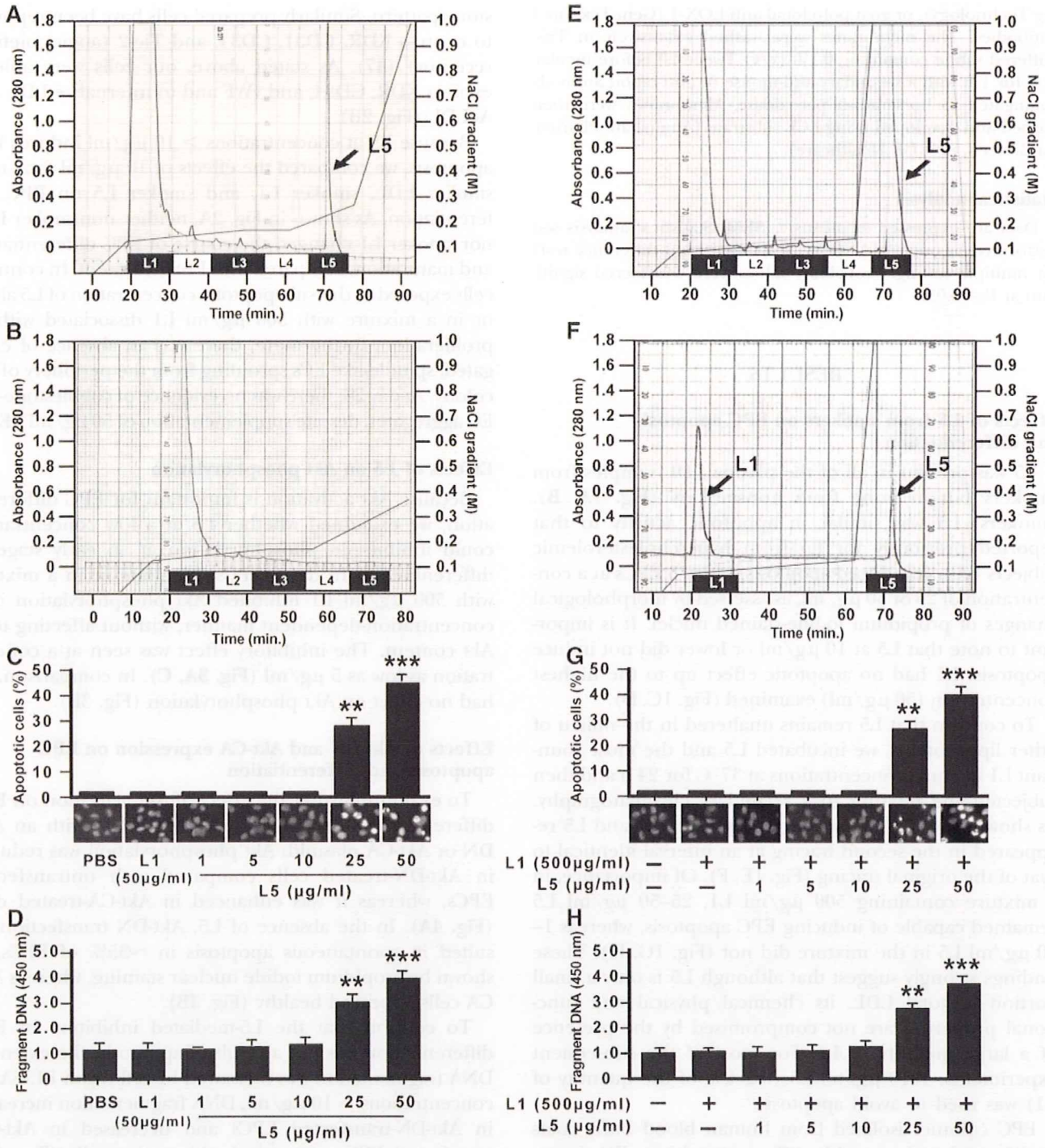

Fig. 1. L1–L5 distribution in smoker and nonsmoker LDL samples and concentration-dependent effects of smoker L5 on endothelial progenitor cell (EPC) apoptosis. A: Ion-exchange chromatogram of a typical LDL fractionation from a chronic smoking subject yields L1–L5. The arrow denotes the L5 peak. B: Chromatogram of LDL fractionation from a healthy, nonsmoking subject lacks L5. C: Evaluation of apoptosis in EPCs after exposure to 50 µg/ml L1 (protein concentration) or increasing doses of L5 (protein concentration) in EBM-2® supplemented with 50 ng/ml vascular endothelial growth factor (VEGF). Cells entering apoptosis appear much brighter because of propidium iodide staining of condensed, fragmented DNA (×20 magnification). D: Cell death ELISA measurement in EPCs after exposure to 50 µg/ml L1 or increasing doses of L5 in EBM-2® supplemented with 50 ng/ml VEGF. E: Appearance of L1–L5 subfractions of another random smoker LDL sample. F: Typical example of "rechromatographic" separation of L1 and L5 after an equal concentration (mmol) mixture of the two subfractions retrieved from L1 and L5 of the subject shown in E. The mixture was incubated for 24 h at 37°C under 5% CO_2 before the second chromatography. G: Assay of EPC apoptosis after exposure to a mixture of 500 µg/ml L1 and 1–50 µg/ml L5 in EBM-2® supplemented with 50 ng/ml VEGF for 24 h. H: ELISA-assessed cell death in EPCs after exposure to a mixture of 500 µg/ml L1 and 1–50 µg/ml L5 for 24 h. ** $P < 0.01$, *** $P < 0.001$ versus PBS (n = 5 for C, D) or no treatment with L1 or L5 (n = 5 for G, H). Values are expressed as mean ± SEM.

JOURNAL OF LIPID RESEARCH

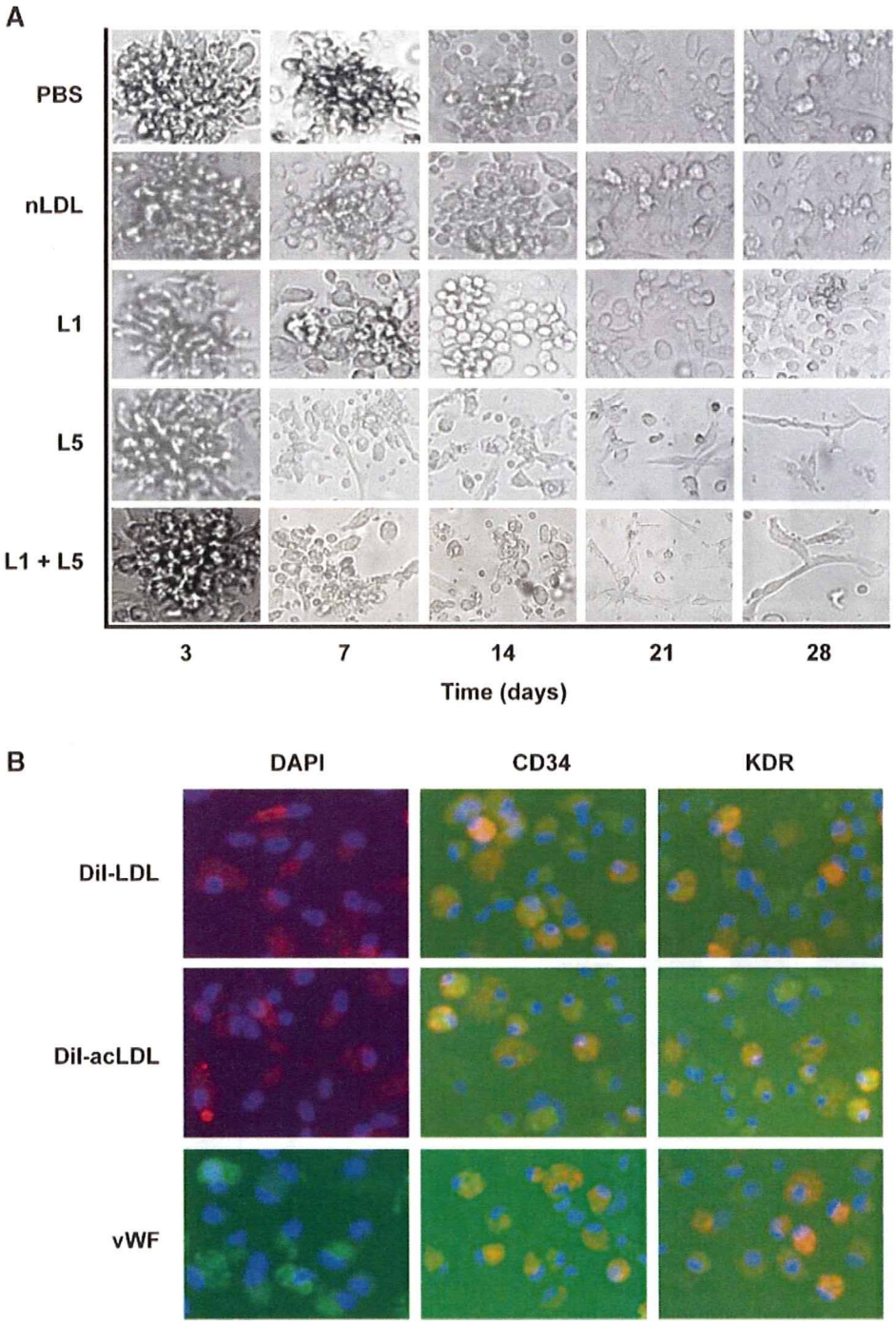

Fig. 2. Morphological and endothelial cell (EC) lineage marker changes in EPC colonies with or without sustained exposure to L5. A: Mononuclear cells were isolated from healthy human blood by density-gradient centrifugation and seeded on 2% gelatin-coated six-well plates in EBM-2® supplemented with VEGF and ascorbic acid. On day 3, when EPC colonies formed, the cells began to be exposed to nonsmoker total LDL, smoker L1, smoker L5 (10 μg/ml each), or a mixture of smoker L1 (500 μg/ml) and L5 (10 μg/ml) in fresh medium with 50 ng/ml VEGF. The treatments were renewed every 3 days, and photomicrographs (×20 magnification) were taken on days 7, 14, 21, and 28. B: Images (×20 magnification) of single and double immunofluorescence stainings exhibiting EC lineage markers CD34 and KDR in healthy differentiating EPCs. Figures are representative of three independent experiments. AcLDL, acetylated low density lipoprotein; DAPI, 4′,6-diamino-phenylindole; DiI, 1,1′-dioctadecyl-3,3,3′,3′-tetramethylindocarbocyanine; vWF, von Willebrand factor.

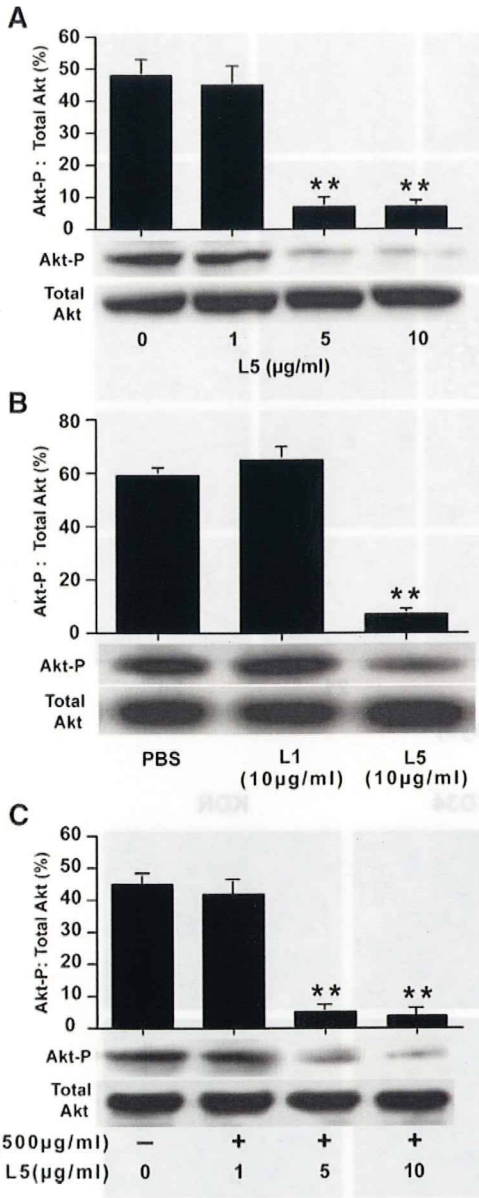

Fig. 3. Effects of L5 on phosphorylated Akt levels in early EPCs. A: EPCs at day 3 were treated with increasing concentrations of L5 for 1 h. Cells were lysed and applied to Western blots to determine the ratio of phosphorylated to total cellular Akt. B: EPCs treated with 10 μg/ml L1 or L5 were subjected to Western blot analysis and compared with respect to Akt phosphorylation (n = 5). C: Akt phosphorylation in EPCs treated with 1–10 μg/ml L5 in the presence of 500 μg/ml L1. ** $P < 0.01$ versus no treatment (A, C; n = 5) or PBS (B). Values are expressed as mean ± SEM.

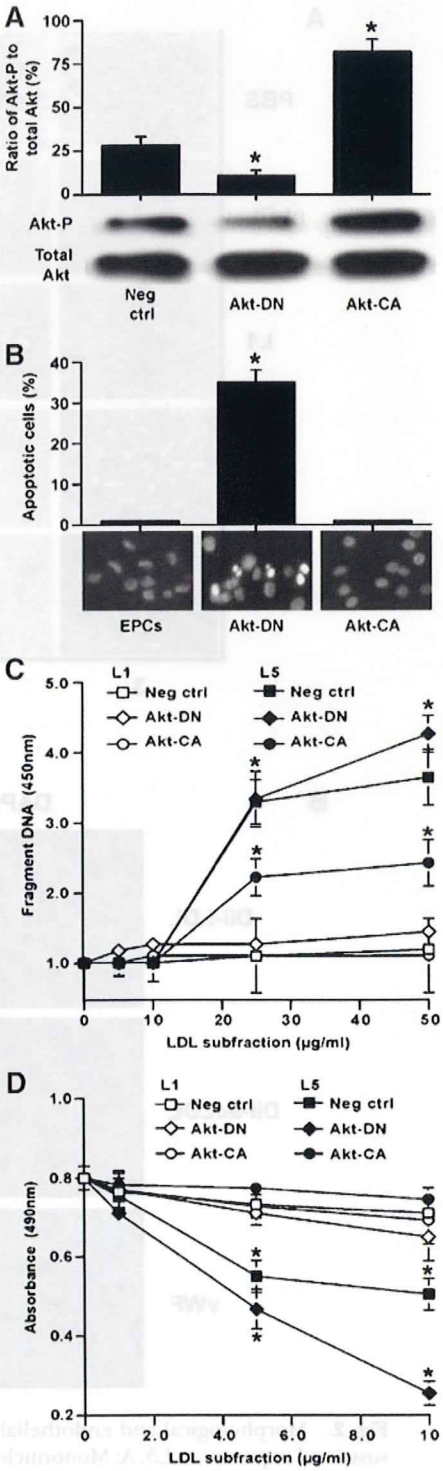

Fig. 4. Effects of Akt plasmid [dominant negative Akt (Akt-DN) or constitutively active Akt (Akt-CA)] transfection on Akt phosphorylation and L5-induced EPC apoptosis. A: Akt-DN or Akt-CA constructs were transfected into EPCs at day 3, as described in Methods. The status of Akt phosphorylation, without L5 treatment, was determined by immunoblotting. B: Fluorescent nuclear staining of EPCs transfected with Akt-DN or Akt-CA. Cells entering apoptosis appear much brighter as a result of propidium iodide staining of condensed, fragmented DNA (×20 magnification). C: Results of cell death ELISA in EPCs transfected with Akt-DN or Akt-CA, followed by treatment with increasing doses of L1 or L5. D: Effects of L5 on mitogenic activity in EPCs transfected with Akt-DN or Akt-CA in a proliferation ELISA assay. * $P < 0.01$ versus EPCs (A, B) or versus the L1 negative control (C, D); n = 5. Values are expressed as mean ± SEM.

(Fig. 4C). In addition, Akt-CA-transfected EPCs showed normal mitogenic activity according to MTS ELISA, even under L5 treatment at 5 and 10 μg/ml (see Fig. 6 below). These data suggest a significant inhibitory effect of L5 on VEGF-induced mitogenic activity of EPCs at day 3.

The effects of Akt-DN and Akt-CA on EPC differentiation were monitored for 28 days after transfection. As early as 6 h after Akt-DN transfection, the EPC colonies started to disintegrate and became fluffy in appearance. The cell number decreased progressively: by day 28, only a few cells remained and no cobblestone-like aggregations were

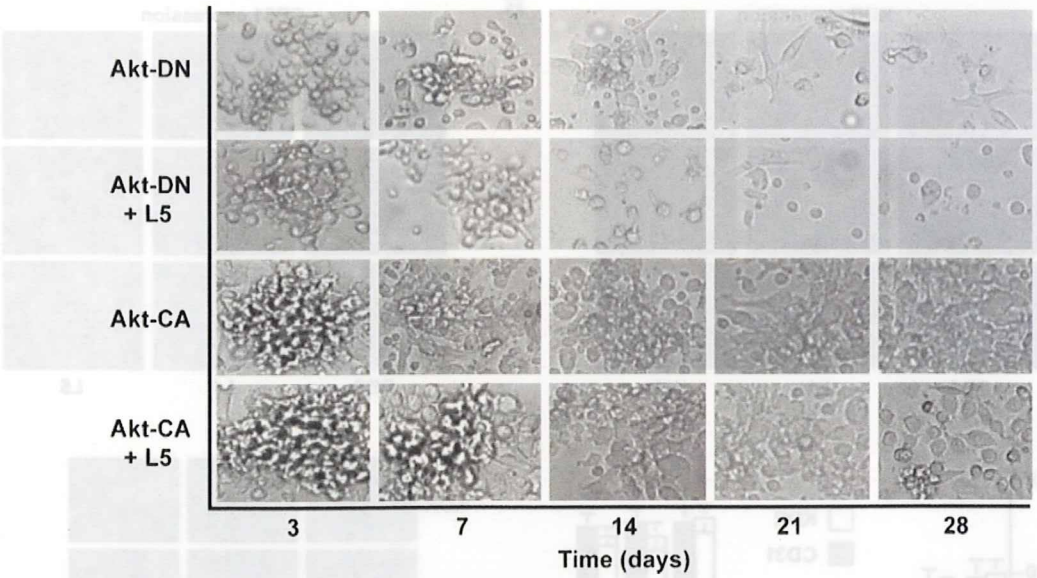

Fig. 5. Morphological changes in Akt-transfected EPCs with or without sustained exposure to L5. Mononuclear cells were isolated from healthy human blood by density-gradient centrifugation and seeded on 2% gelatin-coated, six-well plates in EBM-2® supplemented with VEGF and ascorbic acid. EPC colonies formed at day 3 and were transfected with Akt-DN or Akt-CA; then, 10 μg/ml L5 was added to fresh medium with 50 ng/ml VEGF. The medium was changed every 3 days, and photomicrographs were made at days 7, 14, 21, and 28 to document morphological changes (×20 magnification).

seen. The addition of 10 μg/ml L5 further accelerated EPC colony disassembly, and no mature EPCs were identified (**Fig. 5**). In contrast, EPCs transfected with Akt-CA appeared healthy and differentiated rapidly. By day 28, full-grown cobblestone-like cultures were formed. Akt-CA-transfected EPCs exposed to 10 μg/ml L5 did not impair differentiation. By day 28, mature EPCs formed, although they were not as confluent as in Akt-CA-transfected cells without L5 exposure (Fig. 5).

Effects of Akt-CA and Akt-DN expression on VEGF-induced mitogenic activity in early EPCs

Cell proliferation plays an important role in EPC differentiation. To determine the importance of Akt activation in the mitogenic activity of early EPCs, an MTS assay was performed. Compared with untransfected EPCs, proliferation was suppressed by Akt-DN but supported by Akt-CA. L1 did not affect viability in untransfected EPCs or EPCs transfected with Akt-CA or Akt-DN plasmids (**Fig. 6**). In Akt-CA EPCs, L5 did not hinder VEGF-induced proliferation. However, it did inhibit proliferation in both the untransfected and the Akt-DN-transfected EPCs in a concentration-dependent manner.

Effects of L5 and Akt-DN or Akt-CA transfection on VEGF-induced expression of KDR and CD31 in early EPCs

KDR and CD31, both inducible by VEGF, are EC markers with important functions. KDR transduces VEGF signaling (48). CD31 (platelet-endothelial adhesion molecule 1) promotes adhesion between ECs (49). We examined how L5 inhibits EPC differentiation by affecting the expression of KDR and CD31. In untransfected EPCs, L5 almost completely suppressed the expression of both KDR and CD31 in the setting of supplementation with 50 ng/ml VEGF, whereas L1 (10 and 500 μg/ml) had no effect compared with a PBS control (**Fig. 7A, B, D**). In a physiological mixture of L5 (10 μg/ml) and L1 (500 μg/ml), L5 was still able to inhibit KDR and CD31 expression, whereas 500 μg/ml L1 alone did not (Fig. 7D).

In Akt-DN-transfected EPCs, immunofluorescence emission was reduced for both KDR and CD31, compared with untransfected EPCs. L1 did not exert additional effects, but L5 further suppressed the expression of both markers in Akt-DN EPCs (Fig. 7A, B). In contrast, the expressions of

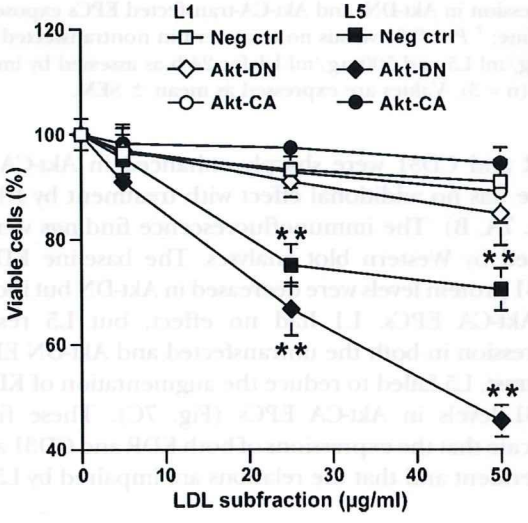

Fig. 6. Viability of Akt-transfected EPCs treated with L1 or L5. EPCs were transfected with Akt-DN or Akt-CA and exposed to increasing concentrations of L1 or L5. ** $P < 0.01$ versus L1 (negative control); n = 5. Values are expressed as mean ± SEM.

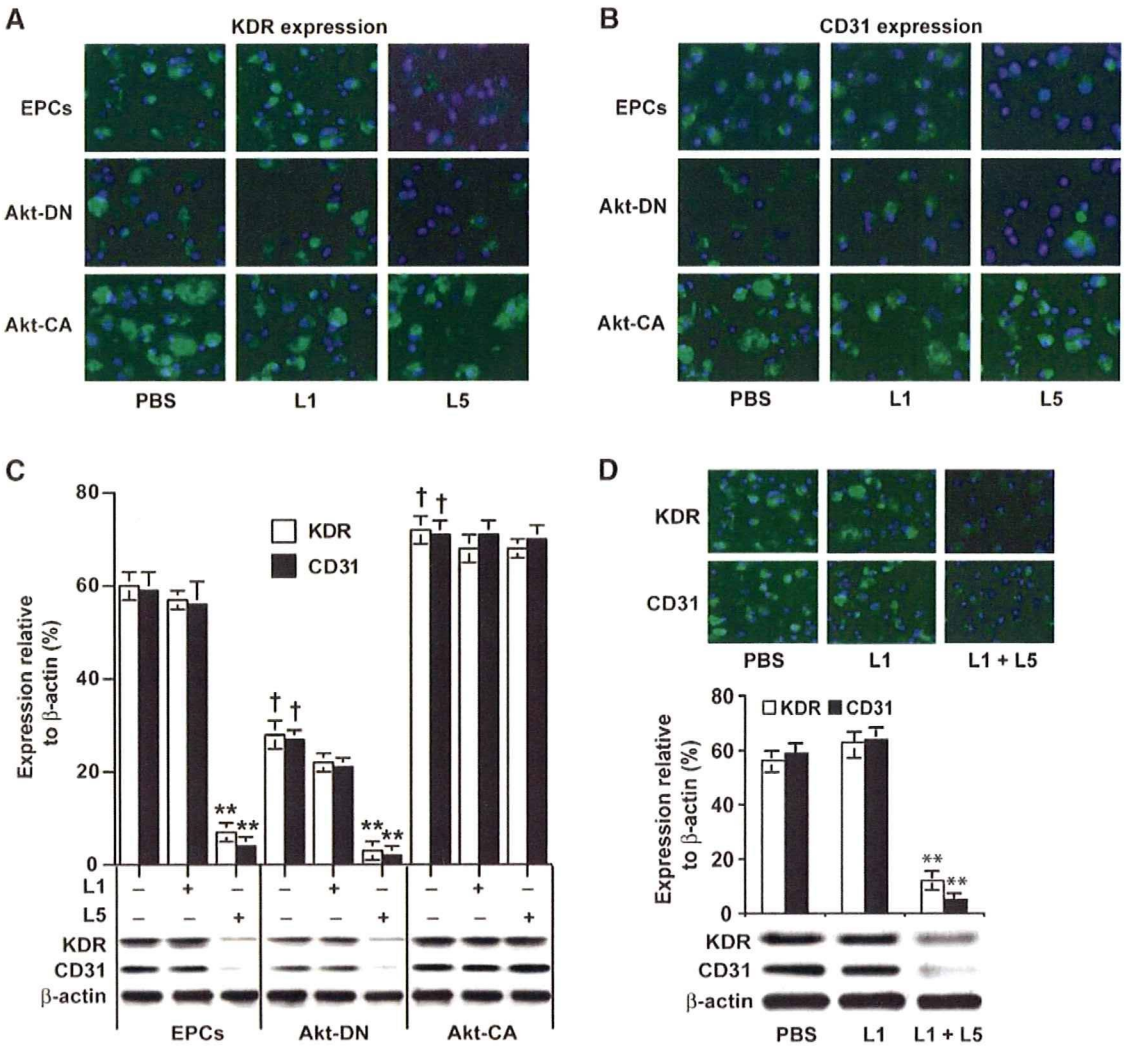

Fig. 7. Effects of L5 on EPC differentiation as measured by KDR and CD31 expression. EPCs transfected with Akt-DN or Akt-CA plasmids were treated with 10 μg/ml L1 or L5 for 24 h in EBM-2® supplemented with 50 ng/ml VEGF. KDR and CD31 expression was detected by immunofluorescence antibody staining with respect to cellular counterstaining. A: KDR immunofluorescence in Akt-DN- and Akt-CA-transfected EPCs treated with 10 μg/ml L1 or L5 (×20 magnification). B: Representative photomicrographs of CD31 immunofluorescence in Akt-DN and Akt-CA EPCs treated with 10 μg/ml L1 or L5 (×20 magnification). C: Western blotting results for KDR and CD31 protein expression in Akt-DN- and Akt-CA-transfected EPCs exposed to 10 μg/ml L1 or L5 for 24 h. ** $P < 0.01$ versus no treatment within each cell line; † $P < 0.01$ versus no treatment in nontransfected EPCs (n = 5). D: KDR and CD31 expression in EPCs treated with a mixture of 10 μg/ml L5 and 500 μg/ml L1 for 24 h as assessed by immunofluorescence antibody staining and Western blotting. ** $P < 0.01$ versus PBS (n = 3). Values are expressed as mean ± SEM.

KDR and CD31 were sharply enhanced in Akt-CA EPCs; there was no additional effect with treatment by L1 or L5 (Fig. 7A, B). The immunofluorescence findings were confirmed by Western blot analyses. The baseline KDR and CD31 protein levels were decreased in Akt-DN but increased in Akt-CA EPCs. L1 had no effect, but L5 restricted expression in both the untransfected and Akt-DN EPCs. In contrast, L5 failed to reduce the augmentation of KDR and CD31 levels in Akt-CA EPCs (Fig. 7C). These findings indicate that the expressions of both KDR and CD31 are Akt-dependent and that the relations are impaired by L5.

Role of LOX-1 in L5 internalization and effect of L5 on LOX-1 expression

To visualize the binding of L5 to the LOX-1 receptor, we prepared DiI-labeled L5 and incubated it with day 3 EPCs. At 10 μg/ml, L5 but not L1 enhanced DiI-L5 binding to EPCs. Pretreatment with 10 μg/ml TS20 abolished DiI-L5 binding (**Fig. 8A**). L1 did not enhance LOX-1 expression in day 3 EPCs, but L5 dose-dependently stimulated LOX-1 expression at both the transcriptional and translational levels (Fig. 8B). Expression of LOX-1 mRNA and of LOX-1 protein was observed in EPCs by day 3; both peaked by day 7 (Fig. 8C). This suggests that monocytes can commit to EPC differentiation as early as day 3 and that the pathway can be blocked by LOX-1 activation by L5. Moreover, LOX-1 internalization of L5 can also be enhanced by L5 in early-stage EPCs, as seen by the increased DiI-L5 staining in EPCs treated with L5. Because the effect was abolished by TS20, a LOX-1-specific neutralizing antibody, and TS20 by itself had no effects on DiI-L5 binding to EPCs, LOX-1 appears to be a critical mediator in the effects of L5 on EPC activity. In

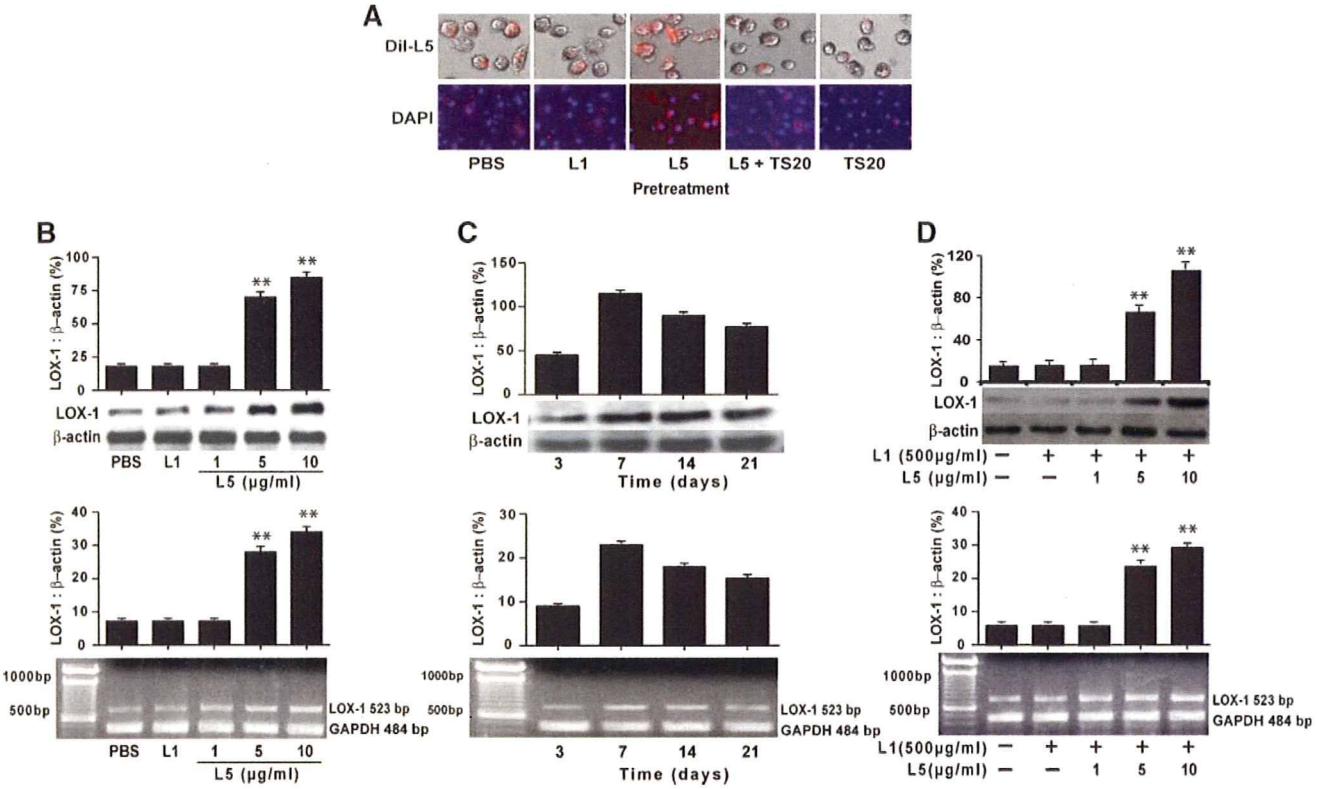

Fig. 8. Role of lectin-like oxidized low density lipoprotein receptor 1 (LOX-1) in L5 internalization and effects of L5 on LOX-1 expression in differentiating EPCs. EPCs were pretreated with TS20 for 1 h after L1 and L5 treatment for 24 h. After medium was removed, cells were treated with DiI-L5 for 6 h. DiI-L5 internalization was confirmed by fluorescence microscopy after cells were washed three times. A: Typical fluorescence microscopy results for DiI-L5 internalization compared with DAPI nuclear staining in early-stage EPCs (×20 magnification). Cells were pretreated with 10 μg/ml L1, L5, or a combination of L5 with 10 μg/ml TS20, followed by DiI-L5. B: Western blot results for LOX-1 mRNA and protein expression in day 3 EPCs exposed to increasing doses of L5. ** $P < 0.01$ versus PBS (n = 5). C: Time course of LOX-1 mRNA and protein expression during EPC differentiation after exposure to 10 μg/ml L5. No significant differences were seen according to time (n = 5). D: Concentration-dependent (1–10 μg/ml) effects of L5 on LOX-1 mRNA and protein expression in day 3 EPCs in a mixture with 500 μg/ml L1. ** $P < 0.01$ versus no treatment (n = 3). Values are expressed as mean ± SEM.

a physiological L5/L1 mixture, L5 was again able to augment LOX-1 expression at both the mRNA and protein levels in a concentration-dependent manner. In contrast, 500 μg/ml L1 by itself had no effect (Fig. 8D).

Akt pathway mediation of L5 inhibitory effects on EPCs

VEGF requires Akt to enhance EPC development, suggesting an essential role of Akt in regulating hematopoietic progenitor cell differentiation (2, 50). Experimental OxLDL has been shown to dose-dependently inhibit phosphorylated Akt in EPCs at day 7 under simultaneous stimulation with VEGF (35). In addition, OxLDL decreased EPC survival, adhesion, migration, and tube formation, effects that were attenuated by pretreatment with a LOX-1 monoclonal antibody (39). To test our hypothesis that L5-stimulated LOX-1 decreases phosphorylated Akt levels, we performed a series of experiments. Fresh mononuclear cells were cultured for 3 days in serum-free EBM-2® and stimulated by L5 in the presence of 50 ng/ml VEGF for 1 h. The cells were lysed and then electrophoretically separated by 10% SDS-PAGE, and immunoblotting was performed with a phosphospecific Akt antibody directed at the Ser^{473} phosphorylation site. As shown in Fig. 3, L5 produced a dose-dependent reduction of phosphorylated Akt in the presence of VEGF, whereas L1 at 10 μg/ml did not inhibit phosphorylated Akt in EPCs (Fig. 3B). Pretreatment of EPCs at day 3 with 10 μg/ml TS20, however, protected against L5-induced reductions of phosphorylated Akt (**Fig. 9**). Likewise, EPC transfection with various Akt constructs showed Akt-DN to decrease phosphorylated Akt, whereas Akt-CA-treated EPCs promoted phosphorylated Akt compared with control EPCs. Moreover, L5 at 10 μg/ml inhibited phosphorylated Akt in control EPCs and in Akt-DN-treated but not Akt-CA-treated EPCs, whereas pretreatment with TS20 prevented L5's inhibitory effects (Fig. 9).

Effects of L5 on EPC senescence and telomerase activity

Some studies have shown that impairment of mitogenic activity in early EPCs by OxLDL can lead to accelerated EPC senescence (36). We used β-galactosidase to detect the acidification typical of the onset of cellular senescence. Extended cultivation of EPCs resulted in an increase of SA-β-gal-positive cells; treatment with L5 accelerated senescence but L1 at those doses had no effect (**Fig. 10A**). By day 3, the proportion of SA-β-gal-positive cells in EPCs treated by L5 at

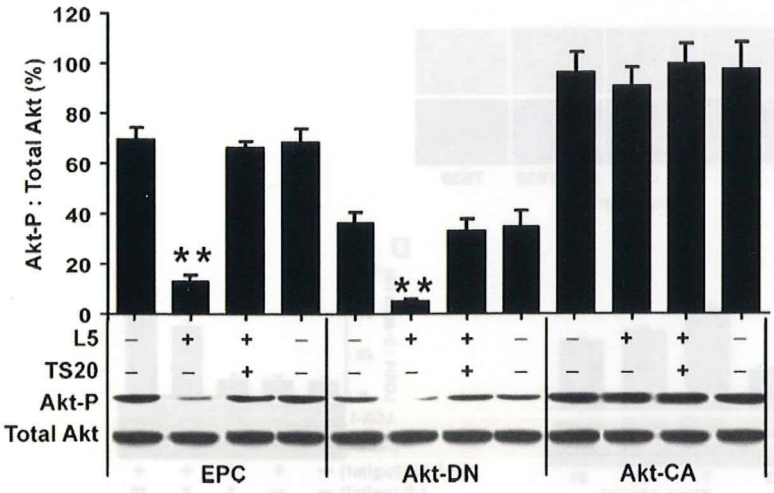

Fig. 9. Akt phosphorylation in Akt-transfected EPCs treated with L5 or L5 and TS20. Akt-DN- and Akt-CA-transfected EPCs were exposed to L5 in the absence or presence of TS20. Akt phosphorylation levels were compared with total Akt levels by Western blot. ** $P < 0.01$ versus negative controls without L5 or TS20 treatment, for L5 versus no treatment in EPCs or for L5 versus no treatment in Akt-DN constructs (n = 5). Values are expressed as mean ± SEM.

10 μg/ml was markedly increased compared with control (Fig. 10B). As noted in Fig. 8, L5 upregulated the expression of LOX-1 in EPCs at day 3. To examine the interplay of L5 and LOX-1 in EPC senescence, we performed further experiments with TS20. The L5-induced increase in SA-β-gal-positive cells was attenuated by 10 μg/ml TS20 (Fig. 10B), suggesting that L5-induced EPC senescence is mediated through the LOX-1 receptor. In addition, SA-β-gal staining showed accelerated senescence of Akt-DN-treated EPCs (Fig. 10A, B), and L5 treatment dramatically increased the effect, with early senescence prevented by TS20. Akt-CA-treated EPCs were strongly resistant to early senescence, maintaining their phenotype regardless of L5 or TS20 treatment. This suggests that L5-induced EPC senescence is mediated through the Akt signal transduction pathway.

Cellular senescence is critically influenced by telomerase, which elongates telomeres, thereby counteracting the telomere length reduction induced by each cell division. It has been demonstrated that proatherosclerosis factors impair telomerase activity in mature ECs (50). Therefore, we measured telomerase activity using the *Telo*TAGGG PCR ELISA^{PLUS} Kit®. Akt-DN EPCs showed decreased telomerase activity compared with the Akt-CA EPC control (Fig. 10C). This effect was exacerbated after treatment with L5. The observed decrease in telomerase activity was attenuated by pretreating cells with TS20, whereas TS20 by itself did not affect EPC senescence or telomerase activity (Fig. 10A–C). Parallel to earlier results, Akt-CA-treated EPC telomerase activity was unaffected by exposure to L5 or TS20.

In the L5/L1 mixture (10:500 μg/ml), L5 maintained its ability to accelerate senescence, as manifested by increased SA-β-gal-positive cells, whereas L1 alone did not (Fig. 10D). Similarly, L5 concentration-dependently inhibited telomerase activity in the presence of L1, whereas L1 by itself did not (Fig. 10E).

DISCUSSION

Our studies demonstrate that L5, a highly electronegative LDL subfraction present in the plasma of smoking subjects, can inhibit the differentiation of EPCs derived from circulating monocytes. This effect was achieved by incubating monocytes with subapoptotic concentrations of L5, which suppressed typical EC markers that were otherwise expressed within 3 days of phenotypic transformation. Furthermore, L5 inhibited EPC telomerase activity, resulting in accelerated senescence. On the basis of our mechanistic studies, we propose that circulating L5 of cigarette smokers activates the LOX-1 receptor, which restricts Akt phosphorylation and other steps necessary to promote normal EPC maturation.

Bone marrow and peripheral blood of adults contain a special subtype of progenitor cells that are able to differentiate into mature ECs. These angiogenic EPCs are a heterogeneous population, derived chiefly from hematopoietic stem cells, and consist of cells at differing stages of maturation (51). Early functional angioblasts, located predominantly in the bone marrow, are characterized by three surface markers: CD133, CD34, and VEGFR2. After migrating to the systemic circulation, EPCs gradually lose their progenitor properties and start to express endothelial markers such as VE-cadherin, endothelial nitric oxide synthase, and vWF (51).

Isolated early peripheral blood-derived EPCs (4–7 days after isolation) represent a small subfraction of mononuclear cells that do not express EC markers. Within several weeks of culture, late-outgrowth cells start to express VE-cadherin and endothelial nitric oxide synthase and acquire a phenotype of mature ECs (4, 50, 52). Gradually, late-outgrowth EPCs functionally form monolayers with a typical cobblestone endothelial appearance (53). An additional feature of isolated EPCs is their ability to incorporate AcLDL and to bind an endothelium-specific lectin (4, 54). Such a smooth transition also may occur in vivo when more immature bone marrow-derived progenitor cells migrate to the systemic circulation. Studies have also shown that human peripheral blood contains pluripotent stem cells as a subset of circulating monocytes (55). These pluripotent monocytic cells can be induced by different culture conditions to acquire different phenotypes (55). Furthermore, it has been shown that monocytes coexpress endothelial markers and form cord-like

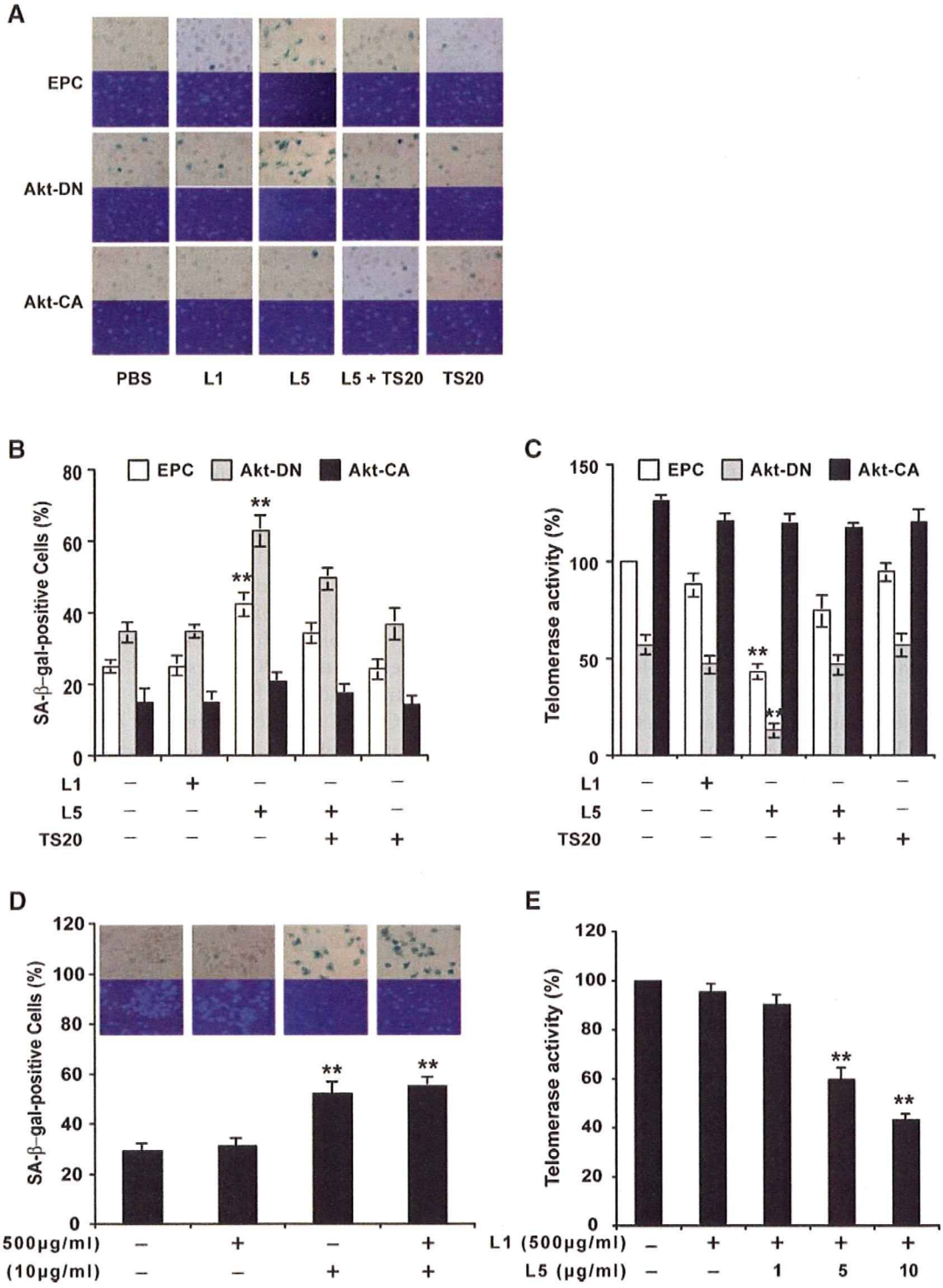

Fig. 10. Effects of L5 on EPC senescence and telomerase activity. EPCs transfected with Akt-DN or Akt-CA constructs were evaluated by β-galactosidase and telomerase assays. A: Representative photomicrographs (×20 magnification) show senescence-associated β-galactosidase (SA-β-gal)-positive cells (blue) in early EPCs treated with 10 μg/ml L1 or L5 with or without 10 μg/ml TS20 pretreatment. For comparison, cells were counterstained with DAPI. B: Percentages of SA-β-gal-positive cells were determined after treatment with L1, L5, a combination of L5 and TS20, or TS20 alone. ** $P < 0.01$ versus no treatment in nontransfected EPCs (n = 5). C: Telomerase activity assay in early L5-treated EPCs and Akt-DN- or Akt-CA-transfected EPCs treated with 10 μg/ml L1 or L5 with or without TS20 pretreatment. Telomerase activity was measured after 24 h of treatment. ** $P < 0.01$ versus no treatment in nontransfected EPCs (n = 5). D: Representative photomicrographs (×20 magnification) and statistical analysis of SA-β-gal-positive cells (blue) in nontreated EPCs and EPCs treated with 500 μg/ml L1, 10 μg/ml L5, or a mixture of L1 and L5. ** $P < 0.01$ versus no treatment (n = 5). E: Telomerase activity assay in early EPCs treated with 1–10 μg/ml L5 in a mixture with 500 μg/ml L1. ** $P < 0.01$ versus no treatment (n = 5). Values are expressed as mean ± SEM.

structures in vitro under angiogenic conditions (56). Thus, ECs may be generated from both $CD14^+$ and $CD14^-$ cells. Ex vivo cultivation of young EPCs from $CD14^+$ or $CD14^-$ mononuclear cells improved neovascularization in a similar manner, whereas freshly purified $CD14^+$ or $CD14^-$ cells without previous culture did not (54). This close relation between monocytic and endothelial lineage cells suggests their possible common origin.

Here, we isolated human mononuclear cells from human blood and plated them on gelatin-coated plates with EC-specific medium supplemented with growth factor mixtures and ascorbic acid. After 3 days of cultivation, early EPC colonies were formed and showed characteristics of ECs, such as internalization of LDL/AcLDL and expression of vWF, VEGFR2/KDR, and CD34, indicating that ECs started differentiation as early as day 3 in culture with special growth factors. Overexpression of Akt-DN inhibited KDR and CD31 expression in EPCs and also blocked EPC proliferation and differentiation (cobblestone EPC formation) induced by VEGF, whereas overexpression of Akt-CA promoted this process, indicating that KDR and Akt signal transduction pathways are crucial elements in the process leading to EPC differentiation induced by VEGF.

It has been suggested that LDL modification may be more important than absolute LDL-cholesterol increase in contributing to atherosclerosis. Previously, we reported that L5, an electronegative LDL subfraction circulating in patients with hypercholesterolemia or type 2 diabetes, can induce marked EC apoptosis (29). Now we report that L5 was present in the LDL of smoking subjects with normal LDL-cholesterol concentrations. In healthy nonsmokers with normal lipid and glucose profiles, L5 is either absent or scanty. We provide evidence that L5 isolated from smoking subjects induces EPC apoptosis in a concentration-dependent manner, whereas sustained exposure to low-dose smoker L5 inhibits EPC proliferation and differentiation without inducing apoptosis. This finding is supported by the observed reduction of CD34- and KDR-positive EPC levels in chronic smokers (6). Our study proved that subapoptotic concentrations of L5 significantly inhibit VEGF-induced KDR and CD31 expression in differentiating EPCs. Resistance to these L5-mediated changes in Akt-CA-treated EPCs suggests that smoker L5 acts in part by decreasing levels of phosphorylated Akt. Indeed, our data demonstrated that L5 inhibits Akt phosphorylation in EPCs at day 3. This is compatible with the observations made with copper-OxLDL, which inhibits VEGF-induced EPC differentiation through dephosphorylation of the Akt kinase on Ser^{473} in EPCs, as reported by Imanishi et al. (35). Akt is a serine-threonine protein kinase that is activated by a number of growth factors and cytokines in a phosphatidylinositol 3-kinase (PI3K)-dependent manner (57). Because VEGF induces EPC differentiation through the phosphatidylinositol 3-kinase-Akt pathway (2), L5 very likely inhibits VEGF-mediated effects by interfering with Akt signaling.

The inhibitory effect of Akt phosphorylation by L5 was abolished by neutralizing LOX-1 with its antibody TS20, indicating that most of L5's signals are transduced by LOX-1. This is supported by the findings that baseline LOX-1 expression, noticeable in day 3 EPCs, was greatly enhanced by L5. Furthermore, internalization of DiI-L5 into EPCs was blocked by TS20, indicative of the mediation role of LOX-1.

Recent studies have demonstrated that atherosclerotic risk factors, including smoking, inversely correlate with the number of differentiated EPCs (6, 14). The proliferation of primary human EPCs is limited by the capacity to divide and the onset of senescence. Loss of telomerase activity has been suggested to constitute the molecular clock that triggers cellular senescence (58). Overexpression of human telomerase reverse transcriptase by adenovirus-mediated gene delivery could lead to a delay of senescence and a recovery/enhancement of the regenerative properties of EPCs (59). We provide evidence that L5 from smokers can accelerate the onset of EPC senescence, which leads to the impairment of proliferative capacity. This is in agreement with the findings by Breitschopf, Zeiher, and Dimmeler (50) that Akt-DN significantly reduces telomerase activity in human umbilical cord ECs. Our experiments showed that the L5-accelerated onset of senescence in EPCs is abolished by TS20. Furthermore, treatment with Akt-DN significantly reduces telomerase activity, whereas Akt-CA prevents the EPC senescence and diminishes telomerase activity induced by L5.

One of the most important observations in this study is that all of L5's adverse effects on differentiating EPCs cannot be compromised in a simulated physiological mixture with the harmless L1. In an L5/L1 ratio of 0.2–10%, L5 remained proapoptotic at higher concentrations (25–50 μg/ml, 5–10% of L1). At subapoptotic concentrations (1–10 μg/ml, 0.2–2% of L1), L5 continued to exert all inhibitory effects on EPCs to halt their differentiation and maturation.

In summary, monocyte differentiation into EPCs starts as early as day 3, as confirmed by the expression of the EPC markers CD31, KDR, and vWF. L5, a highly electronegative LDL found in the plasma of smoking subjects, prematurely terminates EPC differentiation by inhibiting Akt phosphorylation through the LOX-1 receptor signaling pathway. The clinical implications of these in vitro observations are strongly substantiated by the fact that mixing L5 with L1 in physiological ratios does not lessen any of its capacities in the absence of L1. Thus, our findings provide a new insight into the mechanism of smoking-related EPC damage, which may contribute to the impairment of endothelial regeneration and the compensatory neovascularization observed in vivo (60, 61).

This work was supported by a grant from the Philip Morris External Research Program, Research Grant 1-04-RA-13 from the American Diabetes Association, a Pfizer Independent Research Grant (C-H.C.), Grant HL-63364 from the National Institutes of Health, Research Grant 7-03-RA-108 from the American Diabetes Association (C-Y.Y.), and a Postdoctoral Fellowship from the American Heart Association Texas Affiliate (J.P.W.). The authors thank Suzanne Simpson for editorial assistance and Dr. Su Pan for her technical support.

REFERENCES

1. Ross, R. 1993. Atherosclerosis: current understanding of mechanisms and future strategies in therapy. *Transplant. Proc.* **25:** 2041–2043.
2. Dimmeler, S., A. Aicher, M. Vasa, C. Mildner-Rihm, K. Adler, M. Tiemann, H. Rutten, S. Fichtlscherer, H. Martin, and A. M. Zeiher. 2001. HMG-CoA reductase inhibitors (statins) increase endothelial progenitor cells via the PI 3-kinase/Akt pathway. *J. Clin. Invest.* **108:** 391–397.
3. Urbich, C., and S. Dimmeler. 2004. Endothelial progenitor cells functional characterization. *Trends Cardiovasc. Med.* **14:** 318–322.
4. Asahara, T., T. Murohara, A. Sullivan, M. Silver, R. van der Zee, T. Li, B. Witzenbichler, G. Schatteman, and J. M. Isner. 1997. Isolation of putative progenitor endothelial cells for angiogenesis. *Science.* **275:** 964–967.
5. Crosby, J. R., W. E. Kaminski, G. Schatteman, P. J. Martin, E. W. Raines, R. A. Seifert, and D. F. Bowen-Pope. 2000. Endothelial cells of hematopoietic origin make a significant contribution to adult blood vessel formation. *Circ. Res.* **87:** 728–730.
6. Vasa, M., S. Fichtlscherer, A. Aicher, K. Adler, C. Urbich, H. Martin, A. M. Zeiher, and S. Dimmeler. 2001. Number and migratory activity of circulating endothelial progenitor cells inversely correlate with risk factors for coronary artery disease. *Circ. Res.* **89:** E1–E7.
7. Hoetzer, G. L., G. P. Van Guilder, H. M. Irmiger, R. S. Keith, B. L. Stauffer, and C. A. DeSouza. 2007. Aging, exercise, and endothelial progenitor cell clonogenic and migratory capacity in men. *J. Appl. Physiol.* **102:** 847–852.
8. Guven, H., R. M. Shepherd, R. G. Bach, B. J. Capoccia, and D. C. Link. 2006. The number of endothelial progenitor cell colonies in the blood is increased in patients with angiographically significant coronary artery disease. *J. Am. Coll. Cardiol.* **48:** 1579–1587.
9. Schwartzenberg, S., V. Deutsch, S. Maysel-Auslender, S. Kissil, G. Keren, and J. George. 2007. Circulating apoptotic progenitor cells: a novel biomarker in patients with acute coronary syndromes. *Arterioscler. Thromb. Vasc. Biol.* **27:** e27–e31.
10. Loomans, C. J., E. J. de Koning, F. J. Staal, M. B. Rookmaaker, C. Verseyden, H. C. de Boer, M. C. Verhaar, B. Braam, T. J. Rabelink, and A. J. van Zonneveld. 2004. Endothelial progenitor cell dysfunction: a novel concept in the pathogenesis of vascular complications of type 1 diabetes. *Diabetes.* **53:** 195–199.
11. Tepper, O. M., R. D. Galiano, J. M. Capla, C. Kalka, P. J. Gagne, G. R. Jacobowitz, J. P. Levine, and G. C. Gurtner. 2002. Human endothelial progenitor cells from type II diabetics exhibit impaired proliferation, adhesion, and incorporation into vascular structures. *Circulation.* **106:** 2781–2786.
12. Chen, J. Z., F. R. Zhang, Q. M. Tao, X. X. Wang, and J. H. Zhu. 2004. Number and activity of endothelial progenitor cells from peripheral blood in patients with hypercholesterolaemia. *Clin. Sci. (Lond.).* **107:** 273–280.
13. Fujii, H., S. H. Li, P. E. Szmitko, P. W. Fedak, and S. Verma. 2006. C-reactive protein alters antioxidant defenses and promotes apoptosis in endothelial progenitor cells. *Arterioscler. Thromb. Vasc. Biol.* **26:** 2476–2482.
14. Hill, J. M., G. Zalos, J. P. Halcox, W. H. Schenke, M. A. Waclawiw, A. A. Quyyumi, and T. Finkel. 2003. Circulating endothelial progenitor cells, vascular function, and cardiovascular risk. *N. Engl. J. Med.* **348:** 593–600.
15. Michaud, S. E., S. Dussault, P. Haddad, J. Groleau, and A. Rivard. 2006. Circulating endothelial progenitor cells from healthy smokers exhibit impaired functional activities. *Atherosclerosis.* **187:** 423–432.
16. Heeschen, C., J. J. Jang, M. Weis, A. Pathak, S. Kaji, R. S. Hu, P. S. Tsao, F. L. Johnson, and J. P. Cooke. 2001. Nicotine stimulates angiogenesis and promotes tumor growth and atherosclerosis. *Nat. Med.* **7:** 833–839.
17. Heeschen, C., E. Chang, A. Aicher, and J. P. Cooke. 2006. Endothelial progenitor cells participate in nicotine-mediated angiogenesis. *J. Am. Coll. Cardiol.* **48:** 2553–2560.
18. Wang, X., J. Zhu, J. Chen, and Y. Shang. 2004. Effects of nicotine on the number and activity of circulating endothelial progenitor cells. *J. Clin. Pharmacol.* **44:** 881–889.
19. Jaimes, E. A., E. G. DeMaster, R. X. Tian, and L. Raij. 2004. Stable compounds of cigarette smoke induce endothelial superoxide anion production via NADPH oxidase activation. *Arterioscler. Thromb. Vasc. Biol.* **24:** 1031–1036.
20. Raij, L., E. G. DeMaster, and E. A. Jaimes. 2001. Cigarette smoke-induced endothelium dysfunction: role of superoxide anion. *J. Hypertens.* **19:** 891–897.
21. Barua, R. S., J. A. Ambrose, L. J. Eales-Reynolds, M. C. DeVoe, J. G. Zervas, and D. C. Saha. 2001. Dysfunctional endothelial nitric oxide biosynthesis in healthy smokers with impaired endothelium-dependent vasodilatation. *Circulation.* **104:** 1905–1910.
22. Celermajer, D. S., M. R. Adams, P. Clarkson, J. Robinson, R. McCredie, A. Donald, and J. E. Deanfield. 1996. Passive smoking and impaired endothelium-dependent arterial dilatation in healthy young adults. *N. Engl. J. Med.* **334:** 150–154.
23. Wells, A. J. 1994. Passive smoking as a cause of heart disease. *J. Am. Coll. Cardiol.* **24:** 546–554.
24. Tribble, D. L., L. J. Giuliano, and S. P. Fortmann. 1993. Reduced plasma ascorbic acid concentrations in nonsmokers regularly exposed to environmental tobacco smoke. *Am. J. Clin. Nutr.* **58:** 886–890.
25. Alberg, A. J., J. C. Chen, H. Zhao, S. C. Hoffman, G. W. Comstock, and K. J. Helzlsouer. 2000. Household exposure to passive cigarette smoking and serum micronutrient concentrations. *Am. J. Clin. Nutr.* **72:** 1576–1582.
26. Hu, F. B., and W. C. Willett. 2002. Optimal diets for prevention of coronary heart disease. *J. Am. Med. Assoc.* **288:** 2569–2578.
27. Yokode, M., Y. Nagano, H. Arai, K. Ueyama, Y. Ueda, and T. Kita. 1995. Cigarette smoke and lipoprotein modification. A possible interpretation for development of atherosclerosis. *Ann. N. Y. Acad. Sci.* **748:** 294–300.
28. Mahfouz, M. M., S. A. Hulea, and F. A. Kummerow. 1995. Cigarette smoke increases cholesterol oxidation and lipid peroxidation of human low-density lipoprotein and decreases its binding to the hepatic receptor in vitro. *J. Environ. Pathol. Toxicol. Oncol.* **14:** 181–192.
29. Chen, C. H., T. Jiang, J. H. Yang, W. Jiang, J. Lu, G. K. Marathe, H. J. Pownall, C. M. Ballantyne, T. M. McIntyre, P. D. Henry, et al. 2003. Low-density lipoprotein in hypercholesterolemic human plasma induces vascular endothelial cell apoptosis by inhibiting fibroblast growth factor 2 transcription. *Circulation.* **107:** 2102–2108.
30. Asahara, T., H. Masuda, T. Takahashi, C. Kalka, C. Pastore, M. Silver, M. Kearne, M. Magner, and J. M. Isner. 1999. Bone marrow origin of endothelial progenitor cells responsible for postnatal vasculogenesis in physiological and pathological neovascularization. *Circ. Res.* **85:** 221–228.
31. Fulton, D., J. P. Gratton, and W. C. Sessa. 2001. Post-translational control of endothelial nitric oxide synthase: why isn't calcium/calmodulin enough? *J. Pharmacol. Exp. Ther.* **299:** 818–824.
32. Carmeliet, P., M. G. Lampugnani, L. Moons, F. Breviario, V. Compernolle, F. Bono, G. Balconi, R. Spagnuolo, B. Oostuyse, M. Dewerchin, et al. 1999. Targeted deficiency or cytosolic truncation of the VE-cadherin gene in mice impairs VEGF-mediated endothelial survival and angiogenesis. *Cell.* **98:** 147–157.
33. Morales-Ruiz, M., D. Fulton, G. Sowa, L. R. Languino, Y. Fujio, K. Walsh, and W. C. Sessa. 2000. Vascular endothelial growth factor-stimulated actin reorganization and migration of endothelial cells is regulated via the serine/threonine kinase Akt. *Circ. Res.* **86:** 892–896.
34. Llevadot, J., S. Murasawa, Y. Kureishi, S. Uchida, H. Masuda, A. Kawamoto, K. Walsh, J. M. Isner, and T. Asahara. 2001. HMG-CoA reductase inhibitor mobilizes bone marrow-derived endothelial progenitor cells. *J. Clin. Invest.* **108:** 399–405.
35. Imanishi, T., T. Hano, Y. Matsuo, and I. Nishio. 2003. Oxidized low-density lipoprotein inhibits vascular endothelial growth factor-induced endothelial progenitor cell differentiation. *Clin. Exp. Pharmacol. Physiol.* **30:** 665–670.
36. Imanishi, T., T. Hano, T. Sawamura, and I. Nishio. 2004. Oxidized low-density lipoprotein induces endothelial progenitor cell senescence, leading to cellular dysfunction. *Clin. Exp. Pharmacol. Physiol.* **31:** 407–413.
37. Sawamura, T., N. Kume, T. Aoyama, H. Moriwaki, H. Hoshikawa, Y. Aiba, T. Tanaka, S. Miwa, Y. Katsura, T. Kita, et al. 1997. An endothelial receptor for oxidized low-density lipoprotein. *Nature.* **386:** 73–77.
38. Aoki, M., M. Yasutake, and T. Murohara. 2004. Derivation of functional endothelial progenitor cells from human umbilical cord blood mononuclear cells isolated by a novel cell filtration device. *Stem Cells.* **22:** 994–1002.
39. Ma, F. X., B. Zhou, Z. Chen, Q. Ren, S. H. Lu, T. Sawamura, and Z. C. Han. 2006. Oxidized low density lipoprotein impairs endothelial progenitor cells by regulation of endothelial nitric oxide synthase. *J. Lipid Res.* **47:** 1227–1237.

40. Aoyama, T., H. Fujiwara, T. Masaki, and T. Sawamura. 1999. Induction of lectin-like oxidized LDL receptor by oxidized LDL and lysophosphatidylcholine in cultured endothelial cells. *J. Mol. Cell. Cardiol.* **31:** 2101–2114.
41. Mehta, J. L., and D. Y. Li. 1998. Identification and autoregulation of receptor for Ox-LDL in cultured human coronary artery endothelial cells. *Biochem. Biophys. Res. Commun.* **248:** 511–514.
42. Yang, C. Y., J. L. Raya, H. H. Chen, C. H. Chen, Y. Abe, H. J. Pownall, A. A. Taylor, and C. V. Smith. 2003. Isolation, characterization, and functional assessment of oxidatively modified subfractions of circulating low-density lipoproteins. *Arterioscler. Thromb. Vasc. Biol.* **23:** 1083–1090.
43. Ramaswamy, S., N. Nakamura, F. Vazquez, D. B. Batt, S. Perera, T. M. Roberts, and W. R. Sellers. 1999. Regulation of G1 progression by the PTEN tumor suppressor protein is linked to inhibition of the phosphatidylinositol 3-kinase/Akt pathway. *Proc. Natl. Acad. Sci. USA.* **96:** 2110–2115.
44. Imanishi, T., T. Hano, I. Nishio, W. C. Liles, S. M. Schwartz, and D. K. Han. 2000. Transition of apoptotic resistant vascular smooth muscle cells to troptotic sensitive state is correlated with down-regulation of c-FLIP. *J. Vasc. Res.* **37:** 523–531.
45. Dimri, G. P., X. Lee, G. Basile, M. Acosta, G. Scott, C. Roskelley, E. E. Medrano, M. Linskens, I. Rubelj, O. Pereira-Smith, et al. 1995. A biomarker that identifies senescent human cells in culture and in aging skin in vivo. *Proc. Natl. Acad. Sci. USA.* **92:** 9363–9367.
46. Kim, N. W., and F. Wu. 1997. Advances in quantification and characterization of telomerase activity by the telomeric repeat amplification protocol (TRAP). *Nucleic Acids Res.* **25:** 2595–2597.
47. Fiedler, W., R. P. Henke, S. Ergun, U. Schumacher, U. M. Gehling, G. Vohwinkel, N. Kilic, and D. K. Hossfeld. 2000. Derivation of a new hematopoietic cell line with endothelial features from a patient with transformed myeloproliferative syndrome: a case report. *Cancer.* **88:** 344–351.
48. Guo, D., Q. Jia, H. Y. Song, R. S. Warren, and D. B. Donner. 1995. Vascular endothelial cell growth factor promotes tyrosine phosphorylation of mediators of signal transduction that contain SH2 domains. Association with endothelial cell proliferation. *J. Biol. Chem.* **270:** 6729–6733.
49. DeLisser, H. M., P. J. Newman, and S. M. Albelda. 1993. Platelet endothelial cell adhesion molecule (CD31). *Curr. Top. Microbiol. Immunol.* **184:** 37–45.
50. Breitschopf, K., A. M. Zeiher, and S. Dimmeler. 2001. Pro-atherogenic factors induce telomerase inactivation in endothelial cells through an Akt-dependent mechanism. *FEBS Lett.* **493:** 21–25.
51. Blann, A. D., A. Woywodt, F. Bertolini, T. M. Bull, J. P. Buyon, R. M. Clancy, M. Haubitz, R. P. Hebbel, G. Y. Lip, P. Mancuso, et al. 2005. Circulating endothelial cells. Biomarker of vascular disease. *Thromb. Haemost.* **93:** 228–235.
52. Peichev, M., A. J. Naiyer, D. Pereira, Z. Zhu, W. J. Lane, M. Williams, M. C. Oz, D. J. Hicklin, L. Witte, M. A. Moore, et al. 2000. Expression of VEGFR-2 and AC133 by circulating human CD34(+) cells identifies a population of functional endothelial precursors. *Blood.* **95:** 952–958.
53. Gulati, R., D. Jevremovic, T. E. Peterson, S. Chatterjee, V. Shah, R. G. Vile, and R. D. Simari. 2003. Diverse origin and function of cells with endothelial phenotype obtained from adult human blood. *Circ. Res.* **93:** 1023–1025.
54. Urbich, C., C. Heeschen, A. Aicher, E. Dernbach, A. M. Zeiher, and S. Dimmeler. 2003. Relevance of monocytic features for neovascularization capacity of circulating endothelial progenitor cells. *Circulation.* **108:** 2511–2516.
55. Zhao, Y., D. Glesne, and E. Huberman. 2003. A human peripheral blood monocyte-derived subset acts as pluripotent stem cells. *Proc. Natl. Acad. Sci. USA.* **100:** 2426–2431.
56. Schmeisser, A., C. D. Garlichs, H. Zhang, S. Eskafi, C. Graffy, J. Ludwig, R. H. Strasser, and W. G. Daniel. 2001. Monocytes coexpress endothelial and macrophagocytic lineage markers and form cord-like structures in Matrigel under angiogenic conditions. *Cardiovasc. Res.* **49:** 671–680.
57. Datta, S. R., A. Brunet, and M. E. Greenberg. 1999. Cellular survival: a play in three Akts. *Genes Dev.* **13:** 2905–2927.
58. Greider, C. W. 1990. Telomeres, telomerase and senescence. *Bioessays.* **12:** 363–369.
59. Murasawa, S., J. Llevadot, M. Silver, J. M. Isner, D. W. Losordo, and T. Asahara. 2002. Constitutive human telomerase reverse transcriptase expression enhances regenerative properties of endothelial progenitor cells. *Circulation.* **106:** 1133–1139.
60. Chen, C. H., and J. P. Walterscheid. 2006. Plaque angiogenesis versus compensatory arteriogenesis in atherosclerosis. *Circ. Res.* **99:** 787–789.
61. Bochkov, V. N., M. Philippova, O. Oskolkova, A. Kadl, A. Furnkranz, E. Karabeg, T. Afonyushkin, F. Gruber, J. Breuss, A. Minchenko, et al. 2006. Oxidized phospholipids stimulate angiogenesis via autocrine mechanisms, implicating a novel role for lipid oxidation in the evolution of atherosclerotic lesions. *Circ. Res.* **99:** 900–908.

Journal of Cellular Physiology

Oxidative Stress Induces GLUT4 Translocation by Activation of PI3-K/Akt and Dual AMPK Kinase in Cardiac Myocytes

TAKAHIRO HORIE,[1] KOH ONO,[1]* KAZUYA NAGAO,[1] HITOO NISHI,[1] MINAKO KINOSHITA,[1] TERUHISA KAWAMURA,[2] HIROMICHI WADA,[2] AKIRA SHIMATSU,[2] TORU KITA,[1] AND KOJI HASEGAWA[2]

[1]*Department of Cardiovascular Medicine, Graduate School of Medicine, Kyoto University, Kyoto, Japan*

[2]*Division of Translational Research, Kyoto Medical Center, Kyoto, Japan*

In response to metabolic stress, GLUT4, the most abundant glucose transporter, translocates from intracellular vesicles to the plasma membrane. This appears to play an important role in protecting cardiac myocytes from ischemic injury. To investigate the precise mechanisms of GLUT4 translocation in cardiomyocytes, we have established a method for quantifying the relative proportion of sarcolemmal GLUT4 to total GLUT4 in these cells. Stimulation with H_2O_2 resulted in a concentration-dependent increase in GLUT4 translocation, which peaked at 15 min after stimulation. The dominant-negative form (DN) of AMP-activated protein kinase (AMPK) α2 inhibited the H_2O_2-induced translocation of GLUT4. We further examined the role of two known AMPK kinases (AMPKKs), calmodulin-dependent protein kinase kinase (CaMKK)β and LKB1. The DN of CaMKKβ or LKB1 alone inhibited H_2O_2-induced GLUT4 translocation only partially compared to the inhibition produced by the DN of AMPKα2. However, the combination of DN-LKB1 and DN-CaMKKβ inhibited translocation to an extent similar to with DN-AMPKα2. Stimulation with H_2O_2 also activated Akt and the inhibition of PI3-K/Akt prevented GLUT4 translocation to the same extent as with AMPK inhibition. When the DN of AMPKα2 was applied with DN-PI3-K, there was a complete reduction in the GLUT4 membrane level similar to that seen at the 0 time-point. These results demonstrate that AMPK and PI3-K/Akt have an additive effect on oxidative stress-mediated GLUT4 translocation.

J. Cell. Physiol. 215: 733–742, 2008.

GLUT4, the most abundant glucose transporter, resides in intracellular vesicles under basal conditions, and translocates to the plasma membrane in response to insulin, ischemia, and hypoxia (Slot et al., 1991; Fischer et al., 1997). Previous reports have indicated that GLUT4-mediated transport is a major mechanism by which the heart increases glucose uptake during ischemia (Sun et al., 1994). Moreover, hearts from mice with cardiac-selective GLUT4 deficiency develop profound and irreversible systolic and diastolic dysfunction after ischemia and reperfusion (Tian and Abel, 2001). Therefore, the translocation of GLUT4 may represent an important mechanism for protecting against ischemic injury. However, the signaling pathways that mediate GLUT4 translocation in response to metabolic stress are largely unknown.

AMP-activated protein kinase (AMPK) acts as a fuel sensor that is responsible for mediating the cellular adaptation to nutritional and environmental stress (Hardie and Sakamoto, 2006). It is well known that energy deprivation associated with hypoxia and ischemia, exercise, and pressure overload leads to the activation of AMPK in the heart (Tian et al., 2001; Coven et al., 2003; Gonzalez et al., 2004). Recently, several reports have indicated that activation of AMPK, a serine/threonine protein kinase, leads to the translocation of GLUT4 to the cell surface (Li et al., 2004; Yamaguchi et al., 2005). To elucidate the link between metabolic stress and GLUT4 translocation, it is quite important to identify molecular events that occur upstream of AMPK.

Although the identity of the upstream AMPK kinases has proven to be elusive for many years, the tumor suppressor kinase LKB1 was recently shown to be responsible for AMPK kinase activity in the liver (Hawley et al., 2003; Woods et al., 2003). In heart that lacked cardiac muscle LKB1, the activity of AMPKα2 was vastly reduced at the basal level but did not increase in response to ischemia (Sakamoto et al., 2006). However, there appear to be additional pathways that mediate the ischemia-induced activation of AMPK in cardiac muscle (Altarejos et al., 2005; Baron et al., 2005). Recent studies performed in *Saccharomyces cerevisiae* have indicated that AMPK is activated by two upstream kinases that are homologous to the mammalian LKB1 tumor suppressor kinase and calmodulin-dependent protein kinase kinase (CAMKK) (Woods et al., 2005). Another study revealed that CAMKKβ is also likely to activate AMPK in LKB1-deficient cell lines (Hawley et al., 2005). Since CaMKK isoforms are highly expressed in neuronal tissues, it has been suggested that AMPK is controlled by CaMKK rather than LKB1 in Ca^{2+}-regulated pathways in neurons (Hawley et al., 2005). However, it is still unknown whether CaMKKs activate AMPK in cardiomyocytes, which express CaMKK at low levels, under ischemia or oxidative stress.

Since PI3-K/Akt-mediated signal transduction is known to be important for GLUT4 translocation, we also tried to determine whether the PI3-K/Akt pathway is involved in H_2O_2-mediated GLUT4 translocation. Several studies have shown that Akt

Contract grant sponsor: Ministry of Education, Culture, Science, Sports, and Technology of Japan.

*Correspondence to: Koh Ono, Department of Cardiovascular Medicine, Graduate School of Medicine, Kyoto University, 54 Shogoin Kawahara-cho, Sakyo-ku, Kyoto 606-8507, Japan. E-mail: kohono@kuhp.kyoto-u.ac.jp

Received 30 September 2007; Accepted 23 October 2007
DOI: 10.1002/jcp.21353

activation inhibits AMPK (Horman et al., 2006; Soltys et al., 2006). Therefore, these two kinases may interact.

In this study, we focused on the upstream regulatory mechanisms for GLUT4 translocation in cardiomyocytes under oxidative stress. We constructed a GLUT4 reporter vector based on lentiviruses and transduced this gene into neonatal rat cardiomyocytes to precisely measure the ratio of sarcolemmal GLUT4 to total GLUT4 after stimulation. By using this method, we found that AMPK and PI3-K/Akt have an additive effect on oxidative stress-mediated GLUT4 translocation.

Materials and Methods

Reagents

Anti-c-Myc monoclonal antibody (clone 9E10), LY294002 and PD 98059 were purchased from Sigma–Aldrich Co (St. Louis, MO). R-Phycoerythrin (PE)-conjugated AffiniPure F (ab')2 Fragment goat anti-mouse immunoglobulin (IgG) secondary antibody was obtained from Jackson Immmunoresearch (West Grove, PA). Anti-phosphospecific AMPK and Akt antibody and antibodies that recognize both the phosphorylated and total forms of Akt or AMPK were obtained from Cell Signaling (Beverly, MA). GLUT4 antibody (C-20) was obtained from Santa Cruz Biotechnology Inc. (Santa Cruz, CA). Fluo-3 AM, A23187 and 1,2-bis(o-aminophenoxy) ethane-N,N,N,N-tetraacetic acid (BAPTA)-AM were obtained from Molecular Probes (Eugene, OR). Peroxynitrite ($ONOO^-$) was obtained from Calbiochem (San Diego, CA).

Plasmids

DNAs encoding mouse AMPKα2 and CaMKKβ were cloned from mouse heart cDNA (Clontech Laboratories, Inc., Mountain View, CA). The DNAs were amplified using iProof DNA polymerase (Bio-Rad Laboratories, Inc., Hercules, CA) and the sequences were analyzed by an ABI 3100 genetic analyzer. A catalytically inactive mutant of AMPKα2 was made by introducing a mutation of threonine 172 to alanine (T172A) (Stein et al., 2000). A catalytically inactive mutant of CaMKKβ was made by introducing a mutation of aspartic acid 329 to alanine (D329A) (Tokumitsu et al., 2001). A kinase-inactive mutant of LKB1 was made by introducing a mutation of aspartic acid 194 to alanine (D194A) (Woods et al., 2003). A kinase-inactive mutant of PI3-K was provided by Dr. Shioi (Kyoto University, Kyoto) (Shioi et al., 2000). All of these constructs were correctly inserted into a pLenti6/V5-D-TOPO vector (Invitrogen Corp., Carlsbad, CA) to stably express genes in neonatal cardiomyocytes. GLUT4*myc*-GFP reporter gene was constructed by inserting the GLUT4*myc*-GFP fragment of pMX-GLUT4*myc*7-GFP plasmid provided by Dr. Bogan (Harvard Medical School, Boston) into lentivirus vector (Bogan et al., 2001).

Isolation of neonatal rat cardiomyocytes and preparation of lentivirus

The investigation conformed to the *Guide for the Care and Use of Laboratory Animals* published by the US National Institutes of Health (NIH Publication No. 85-23, revised 1996). Primary neonatal rat ventricular cardiomyocytes were prepared as previously described (Hasegawa et al., 1997). We produced lentiviral stocks in 293FT cells following the manufacturer's protocol (Invitrogen).

Subcellular fractionation

Four 10-cm plates of neonatal rat cardiomyocytes were used per condition to isolate low-density microsomal and plasma membrane fractions. Subcellular fractionation was performed as described previously (Bogan et al., 2001).

Measurement of the translocation of GLUT4 in the plasma membrane by flow cytometry

Two days after transduction of the GLUT4 reporter gene, cells were starved in DMEM without fetal bovine serum for 3 h before stimulation. After an appropriate time after stimulation, cells were quickly transferred to 4°C and washed with cold phosphate-buffered saline (PBS). All steps were carried out at 4°C, and externalized *myc*-epitope was stained on adherent cells. Cells were incubated with a 1:300 dilution of anti-Myc (9E10) antibody in PBS-2% bovine serum albumin (BSA)-4% goat serum for 1 h. Cells were washed twice in cold PBS and incubated with a 1:300 dilution of PE-conjugated goat F(ab')2 anti-mouse IgG secondary antibody in PBS-2% BSA-4% goat serum for 0.5 h. Cells were washed four times in cold PBS and resuspended by gentle scraping in PBS-2% BSA. Flow cytometry was performed on a FACS Aria (BD Biosciences, San Jose, CA). Appropriate compensation between FITC and PE was set using uninfected (GFP negative) cells or cells stained only with PE. For each sample, data were collected from >10,000 cells. We used median fluorescence intensities for quantification, since this measure of central tendency is least sensitive to outliers. For each sample, the PE and GFP fluorescences specifically attributable to the presence of the GLUT4 reporter were determined by subtracting background fluorescences, measured using control unstained cells and cells that did not express the reporter, respectively. The ratio of fluorescence intensities (PE/FITC) was used to determine the cell-surface/total GLUT4 ratio.

Glucose uptake assays

Cardiomyocytes were grown in 24-well plates. 2-Deoxyglucose (2DG) uptake was determined by the method of Moyers et al. (1996). 2-Deoxy-D-[1-^{3}H]glucose was obtained from Amersham Biosciences Corp., Piscataway, NJ.

Flow cytometric analysis of Ca^{2+}

Changes in intracellular free ionized calcium concentrations ([Ca2+]i) were measured using the fluorescent calcium indicator fluo-3 acetoxymethyl ester (fluo-3-AM) as previously described (Ono et al., 2001).

Measurement of ATP and AMP in cardiomyocytes by an HPLC-based method

Culture medium was removed by aspiration, and ice-cold 0.4 M perchloric acid (500 μl per 1,000,000 cells) was then added immediately. Nucleotides were extracted and separated by reversed-phase HPLC (Amersham Biosciences) using a phosphate-buffered acetonitrile gradient mobile phase to measure AMP, ADP, and ATP (Manfredi et al., 2002).

Statistics

Data are presented as means ± SE. Statistical analyses were performed using analysis of variance and a Bonferroni post-test in Figures 2E and 5E. Statistical comparisons were performed using unpaired *t* tests in Figures 3, 4, and 5B. Statistical significance was accepted at a *P* value of less than 0.05.

Results

Assays for changes in the proportion of GLUT4 at the plasma membrane

A GLUT4 reporter containing Myc epitope tags in the first exofacial loop as well as GFP fused in-frame at the carboxy terminus was expressed in cardiomyocytes by a lentivirus system. We could transduce this reporter gene to more than 90% of cardiomyocytes (Fig. 1A). As shown in Figure 1B, stimulation with 10 μg/ml insulin for 10 min induced the rapid translocation of GLUT4 to the plasma membrane, which was detected by an anti-Myc monoclonal antibody and a PE-conjugated secondary antibody (upper two pictures). Green fluorescence indicates the total amount of the reporter present in each cell (lower pictures). We also used differential centrifugation to isolate microsomal and plasma membrane

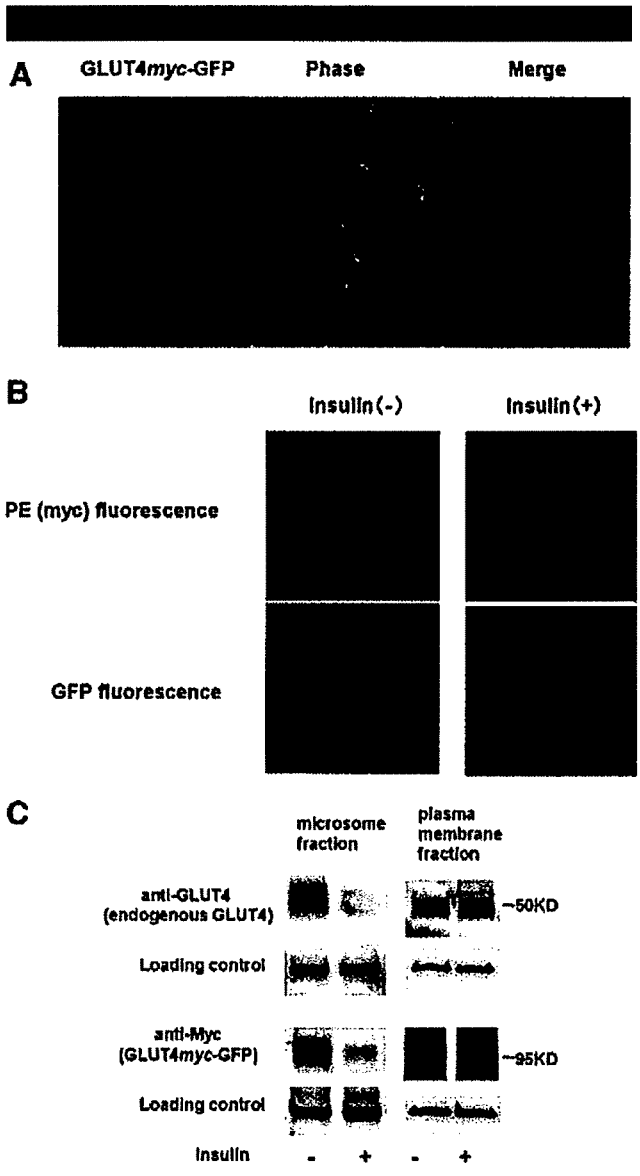

Fig. 1. Insulin triggers the translocation of GLUT4 from an intracellular location to the plasma membrane of cardiomyocytes. A: Expression of GLUT4*myc*-GFP reporter gene in neonatal rat ventricular cardiomyocytes. GLUT4*myc*-GFP was transduced into cells with lentivirus as described (Materials and Methods Section). GFP fluorescence represents expression of the reporter. B: Neonatal rat ventricular cardiomyocytes expressing GLUT4*myc*-GFP were stimulated with or without insulin for 10 min. Stimulation with 10 μg/ml insulin externalized Myc epitope tag which was detected by an anti-Myc monoclonal antibody and a PE-conjugated secondary antibody (upper pictures). GFP fluorescence represents the total amount of the reporter present in a cell (lower pictures). C: Microsome fraction and plasma membrane fractions were isolated and analyzed by SDS–PAGE and immunoblotting. Immunoblotting was performed using an antibody directed against the carboxyl terminus of GLUT4 and revealed that both the reporter (95 kDa) and native GLUT4 (50 kDa) are redistributed from the microsome fraction to the plasma membrane after insulin treatment.

fractions from cells expressing the GLUT4*myc*-GFP reporter and from control cells. As shown in Figure 1C, acute treatment with insulin caused similar decreases in the amounts of both native GLUT4 (~50 kDa) and the reporter protein (~95 kDa) in the microsome fraction. Correspondingly, insulin treatment caused similar increases in both proteins in the plasma membrane fraction. Thus, both the reporter and endogenous GLUT4 proteins redistribute to the plasma membrane in a similar manner.

H_2O_2 induces a rapid translocation of GLUT4

As shown in Figure 2A, stimulation with 100 μM H_2O_2 for 15 min also induced the rapid translocation of GLUT4 to the plasma membrane, which was detected by an anti-Myc monoclonal antibody and a PE-conjugated secondary antibody (upper two pictures). Green fluorescence indicates the total amount of the reporter present in each cell (lower pictures). To precisely measure H_2O_2-stimulated GLUT4 externalization in primary neonatal cardiomyocytes, serum-starved cells expressing the GLUT4*myc*-GFP reporter were treated or not with H_2O_2 and stained for externalized Myc epitope tag, which was analyzed by FACS as described in the Materials and Methods Section (Fig. 2B). This technique allows the simultaneous measurement of PE fluorescence (corresponding to cell-surface GLUT4 reporter and shown on the vertical scale) and GFP fluorescence (corresponding to total GLUT4 reporter and shown on the horizontal scale). Control cardiomyocytes that do not express the reporter (shown in light blue) have background fluorescences that are highly correlated across the relevant wavelengths and appear as a diagonal population. For cells expressing the reporter but which are not stained for cell-surface Myc epitope (shown in light green), fluorescence along the PE axis is due entirely to this background autofluorescence. Control experiments using secondary antibody without primary (anti-Myc) antibody, as well as control experiments using both primary and secondary antibodies on cells that did not express the reporter, demonstrated that background staining is negligible (data not shown); thus, essentially all of the increase in PE fluorescence observed in the basal (blue) and H_2O_2-stimulated (red) populations is due to the detection of Myc on the cell surface. The distribution of each of the stained populations (basal and H_2O_2-stimulated, shown in blue and red, respectively) falls along a diagonal because the amount of Myc epitope at the surface of each cell is proportional to the amount of the reporter present within the cell. As shown in Figure 2C, the cell-surface/total GLUT4 ratio rapidly increased after stimulation with 100 μM H_2O_2 and peaked at 15 min to an extent similar to that induced by 10 μg/ml of insulin for 10 min. Concentration-dependent changes in GLUT4 translocation were also examined. H_2O_2 at both 100 and 500 μM had similar effects on the translocation of GLUT4 after 15 min of stimulation (Fig. 2D). Next, we evaluated whether H_2O_2 induces 2DG uptake in cardiomyocytes. As shown in the previous experiments by Morisco et al. (2005), insulin stimulation induced 2DG uptake to almost twice that in the control. Treatment with H_2O_2 at 100 μM had maximal effects on 2DG uptake. However, the increases in 2DG uptake were not as large as that obtained with insulin stimulation (Fig. 2E).

CaMKKβ and LKB1 are required for H_2O_2-induced GLUT4 translocation upstream of AMPK

To test whether AMPK is involved in H_2O_2-induced GLUT4 translocation, a dominant-negative mutant of AMPKα2 (DN-AMPKα2) was expressed in cardiomyocytes by lentivirus. Expression of DN-AMPKα2 significantly inhibited the cell-surface/total GLUT4 ratio at 15 and 25 min after stimulation with 100 μM H_2O_2 (Fig. 3A). Figure 3B shows that the expression of DN-AMPKα2 inhibited the H_2O_2-induced phosphorylation of AMPK. We further examined the upstream signaling cascade of AMPK. The CaMKK inhibitor STO-609 inhibited H_2O_2-induced GLUT4 translocation at 15 min after stimulation (data not shown). Expression of a dominant-negative mutant of CaMKKβ (DN-CaMKKβ) inhibited GLUT4 translocation significantly only at 15 min after

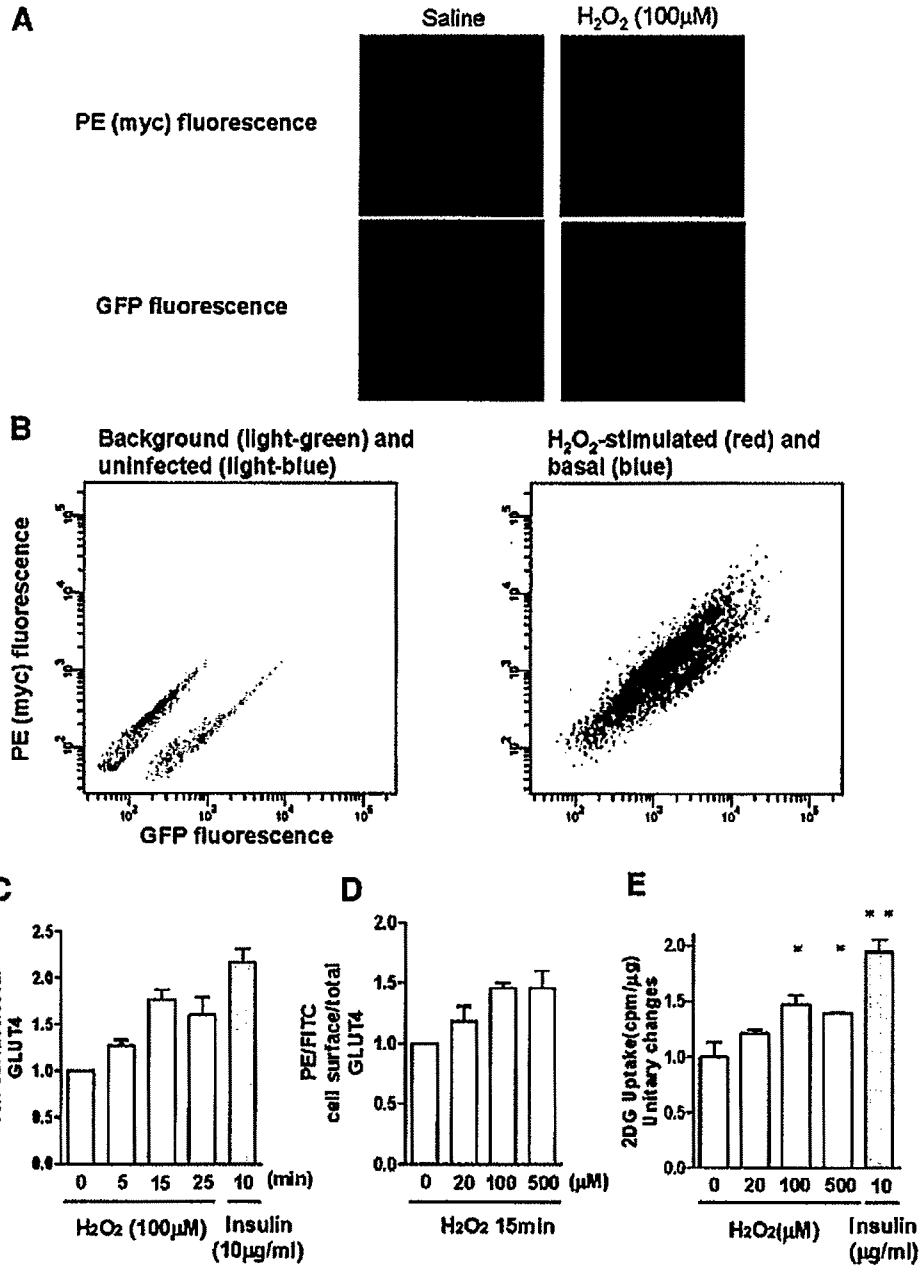

Fig. 2. Assays for changes in the proportion of GLUT4 at the plasma membrane by stimulation with H_2O_2. A: Stimulation with 100 μM H_2O_2 for 15 min induced the rapid translocation of GLUT4 to the plasma membrane, which was detected by an anti-Myc monoclonal antibody and a PE-conjugated secondary antibody (upper two pictures). Green fluorescence indicates the total amount of the reporter present in each cell (lower pictures). B: Flow cytometry was used to measure H_2O_2-stimulated GLUT4 translocation in primary neonatal cardiomyocytes. Control cardiomyocytes that do not express the reporter are shown in light blue. Cells expressing the reporter but which are not stained for cell-surface Myc epitope are shown in light green. The increase in PE fluorescence observed in the basal (blue) and H_2O_2-stimulated (red) populations is due to the detection of Myc on the cell surface. C: Time-dependent change in GLUT4 translocation induced by H_2O_2. The level of GLUT4 translocation without treatment was set at 1.0. Values are the means ± SE of four to eight independent experiments. D: Concentration-dependent change in GLUT4 translocation induced by H_2O_2. The level of GLUT4 translocation without treatment was set at 1.0. Values are the means ± SE of four to eight independent experiments. E: 2DG uptake induced by insulin or H_2O_2. The mean level of 2DG uptake without treatment was set at 1.0. Values are the means ± SE of four independent experiments.

stimulation (Fig. 3C). Figure 3D shows that the expression of DN-CaMKKβ inhibited the H_2O_2-induced phosphorylation of AMPK. We also examined another upstream kinase, LKB1 tumor suppressor kinase, for the activation of AMPK. Expression of a dominant-negative mutant of LKB1 (DN-LKB1) significantly inhibited GLUT4 translocation only at 25 min after stimulation (Fig. 3E). Figure 3F shows that the expression of DN-LKB1 inhibited the H_2O_2-induced phosphorylation of AMPK. However, when both DN-CaMKKβ and DN-LKB1 were expressed at the same time, H_2O_2-induced GLUT4 translocation was significantly inhibited at 5, 15, and 25 min after stimulation (Fig. 3G). Figure 3H shows that the expression of

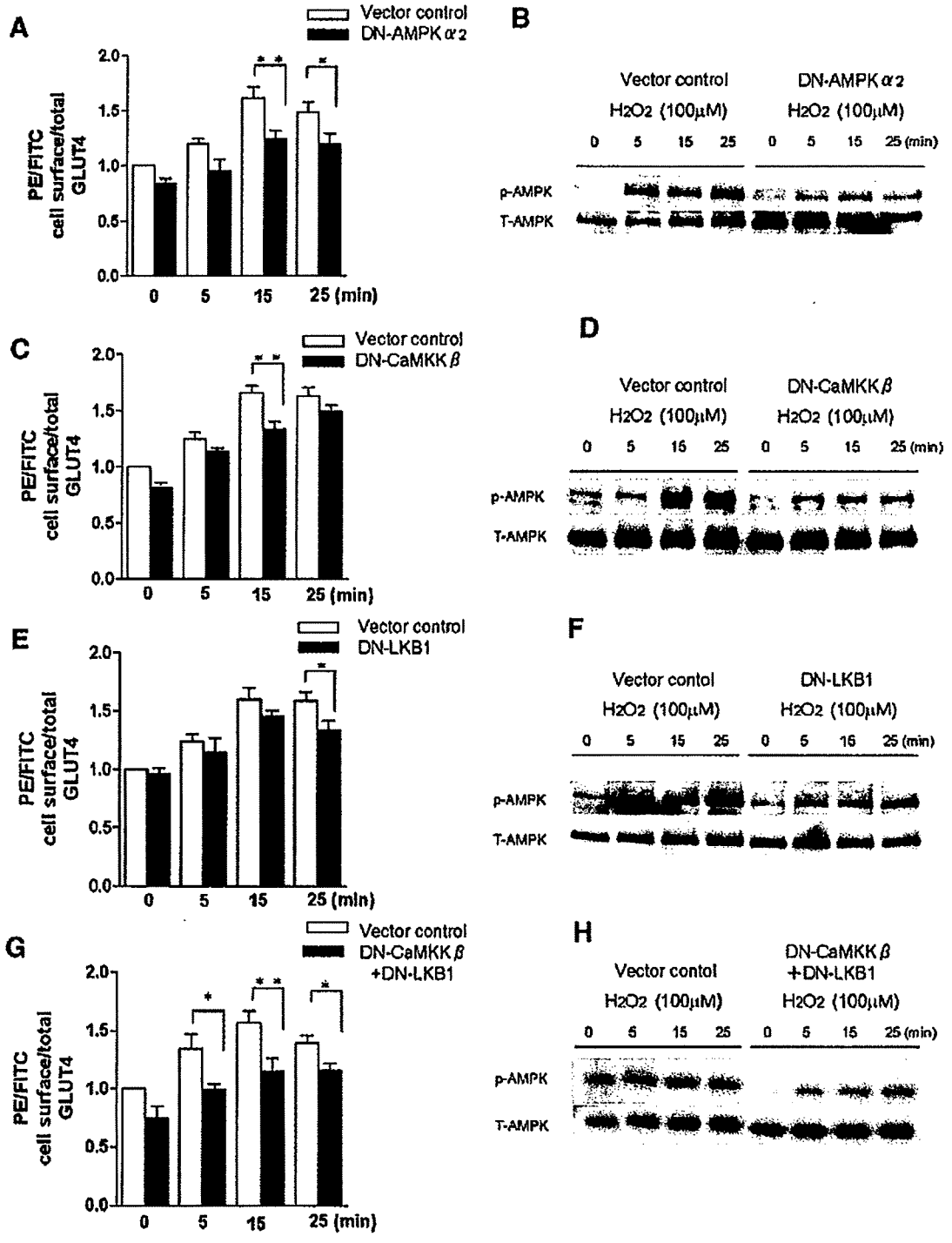

Fig. 3. Effect of the inhibition of AMPK and two kinases upstream of AMPK. The translocation of GLUT4 in the plasma membrane was measured by flow cytometry as described in the Materials and Methods Section. The level of GLUT4 translocation without treatment was set at 1.0. Values are the means ± SE of four to eight independent experiments. A: Dominant-negative AMPKα2 (DN-AMPKα2) inhibited H_2O_2-induced GLUT4 translocation as measured by FACS analysis at 15 and 25 min after exposure to H_2O_2 ($^*P<0.05$, $^{**}P<0.01$). B: Western blot analysis indicated that H_2O_2-induced AMPK activation was reduced by the expression of DN-AMPKα2. C: Dominant-negative CaMKKβ (DN-CaMKKβ) inhibited H_2O_2-induced GLUT4 translocation as measured by FACS analysis only at 15 min after exposure to H_2O_2 ($^{**}P<0.01$). D: H_2O_2-induced AMPK activation was inhibited by the expression of DN-CaMKKβ. E: Dominant-negative LKB1 (DN-LKB1) inhibited H_2O_2-induced GLUT4 translocation as measured by FACS analysis only after 25 min of exposure to H_2O_2 ($^*P<0.05$). F: H_2O_2-induced AMPK activation was reduced by the expression of DN-LKB1. G: DN-CaMKKβ and DN-LKB1 additively inhibited H_2O_2-induced GLUT4 translocation as measured by FACS analysis ($^*P<0.05$, $^{**}P<0.01$). H: H_2O_2-induced AMPK activation was reduced by the expression of both DN-CaMKKβ and DN-LKB1.